Supplementary Information

Disentanglement of Excited-State Dynamics with Implications for FRET Measurements: Two-Dimensional Electronic Spectroscopy of a BODIPY-Functionalized Cavitand

John P. Otto,[a,‡] Lili Wang,[a,‡] Igor Pochorovski,[b] Samuel M. Blau,[c] Alán Aspuru-Guzik,[c,d] Zhenan Bao,[b,*] Gregory S. Engel,[a,*] Melanie Chiu[b,†,*]

[a] Department of Chemistry, University of Chicago, Chicago, IL 60637

[b] Department of Chemical Engineering, Stanford University, Stanford, CA 94305

[c] Department of Chemistry and Chemical Biology, Harvard University, Cambridge, MA 02138

[d] Senior Fellow, Canadian Institute for Advanced Research, Toronto, Ontario M5G 1Z8, Canada

[*] To whom correspondence should be addressed: zbao@stanford.edu, gsengel@uchicago.edu, and melanie.chiu@stonybrook.edu

[‡] These authors contributed equally to this work.

[†] Current address: Department of Chemistry, Stony Brook University, Stony Brook, NY 11794

Table of Contents

S1. Synthesis Information

S1.1. Synthesis Scheme

Scheme S1. Synthesis of BODIPY-dye-substituted cavitand 1.

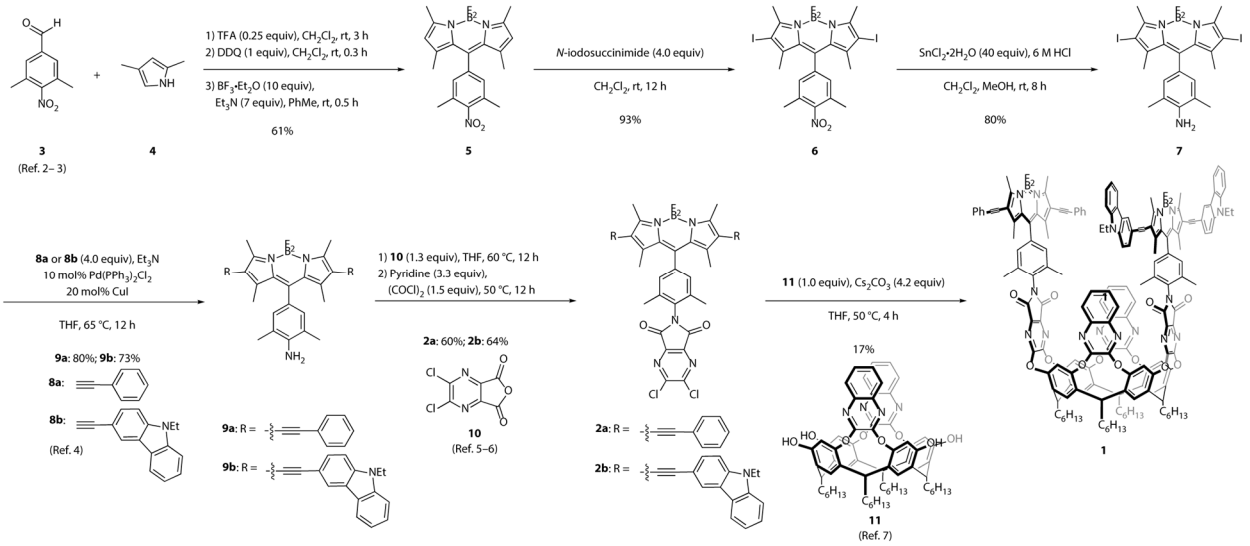

S1.2. Materials and General Methods

Compound names were generated using ChemDraw 15 software. All chemicals were purchased at reagent grade from Acros Organics, TCI Chemicals, Sigma Aldrich, or Strem Chemicals and used without further purification. "Oven-dried" glassware was dried at 110 °C for at least 12 h before use. Tetrahydrofuran (THF), toluene, and CH_2Cl_2 were dried according to published procedures.[1] Triethylamine and pyridine were distilled from CaH_2 and deoxygenated prior to use. Flash chromatography (FC) was performed using SiO_2 (60 Å, 0.040–0.063 mm, Sorbent Technologies) and thin-layer chromatography (TLC) was performed using glass-backed plates (60 Å, hard layer, with 254 nm fluorescent indicator, Sorbent Technologies). ^{1}H, ^{13}C, and ^{19}F NMR spectra were recorded on a Varian Inova 300, Varian Mercury 400, Varian AS 400, or Varian Inova 500 spectrometer. Spectra were recorded at 298 K unless otherwise noted; residual solvent peaks were used as internal references or tetramethylsilane was used as an external reference. Apparent resonance multiplicities are described as s (singlet), br s (broad singlet), d (doublet), t (triplet), q (quartet), m (multiplet), and br m (broad multiplet). Deuterated solvents were purchased from Cambridge Isotopes and used as received. UV/Vis spectra were recorded using a Cary 6000i UV/Vis/NIR spectrometer and a standard 3.5 mL quartz cell (4 optical windows) with a 10 mm path length at 293 K. The absorption maxima (λ_{max}) are reported in nm with the molar extinction coefficient (ε) in M^{-1} cm^{-1} in

parentheses; shoulders are indicated as sh. Mass spectrometry was performed by the Mass Spectrometry Service at the University of Florida, Gainesville or at the Mass Spectroscopy Facility at University of Chicago. High-resolution matrix-assisted laser desorption ionization (HR-MALDI-TOF) mass spectra were recorded on a Bruker Microflex LRF MALDI-TOF spectrometer using dithranol (DTL) as matrix (University of Florida). High-resolution electrospray ionization (HR-ESI-TOF) mass spectra were recorded on an Agilent 6220-ESI-TOF (University of Florida) or Agilent 6224-TOF-MS (University of Chicago) mass spectrometer. High-resolution atmospheric pressure chemical ionization (HR-APCI-TOF) mass spectra were recorded on an Agilent 6200-APCI-TOF (University of Florida). Isotope peaks with the highest relative abundance are reported.

S1.3. Synthesis Procedures

Compounds **4** and **8a** are commercially available and were used as received. Compounds **3**,[2-3] **8b**,[4] and **10**,[5-6] and **11**[7] are known and were prepared according to literature procedures.

10-(3,5-dimethyl-4-nitrophenyl)-5,5-difluoro-1,3,7,9-tetramethyl-5*H*-4λ^4,5λ^4-dipyrrolo[1,2-*c*:2',1'-*f*][1,3,2]diazaborinine (5).

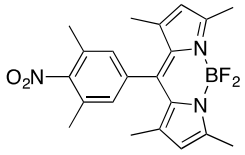

To a solution of 2,6-dimethyl-4-nitro-benzaldehyde (7.10 g, 39.4 mmol, 1.00 equiv) and 2,4-dimethylpyrrole (8.10 mL, 78.8 mmol, 2.00 equiv) in CH_2Cl_2 (2.00 L) in a flame-dried, round-bottomed flask, trifluoroacetic acid (0.78 mL, 10.2 mmol, 0.26 equiv) was added dropwise. The resulting solution was stirred at rt for 3 h under N_2, during which, the solution changed from a clear and pale yellow to clear and bright orange, and was monitored by TLC (SiO_2; CH_2Cl_2/hex 2:1) for the consumption of 2,6-dimethyl-4-nitro-benzaldehyde. A solution of DDQ (8.94 g, 39.4 mmol, 1.00 equiv) in CH_2Cl_2 (1.00 L) was added slowly to the reaction mixture, and the resulting, cherry-red, clear solution was stirred under ambient atmosphere for 20 min. The organic solution was washed with water, dried over $MgSO_4$, filtered, and concentrated to dryness in vacuo. The orange residue was suspended in toluene (2.00 L) under a nitrogen atmosphere and the suspension was de-gassed by bubbling N_2 for 15 min. Et_3N (38.0 mL, 272 mmol, 6.90 equiv), followed by $BF_3 \bullet Et_2O$ (49.5 mL, 396 mmol, 10.1 equiv) were added to the orange suspension via addition funnel. The resulting dark brown suspension was stirred for 30 min at rt, then washed with water (3 x 2.00 L). The organic layer was dried over $MgSO_4$, filtered, and concentrated in vacuo. The crude product was purified by FC (SiO_2; CH_2Cl_2/hex 1:1) and recrystallization (CH_2Cl_2/hexanes) to afford **5** (9.54 g, 24.0 mmol, 61%) as blocky, bright orange crystals. R_f = 0.40 (SiO_2,

CH_2Cl_2/hexanes 1:1); ^{1}H NMR (400 MHz, CDCl3): δ = 7.11 (s, 2H, ArH), 6.01 (s, 2H, PyrH), 2.55 (s, 6H, CH_3), 2.38 (s, 6H, CH_3), 1.44 ppm (s, 6H, CH_3); ^{13}C NMR (101 MHz, $CDCl_3$): δ = 156.4 (C_{Ar}), 152.3 (C_{Ar}), 142.9(C_{Ar}), 139.3 (C_{Ar}), 137.3 (C_{Ar}), 131.2 (C_{Ar}–H), 128.9 (C_{Ar}–H), 121.8 (C=C), 17.8 (CH_3), 15.1 (CH_3), 14.9 ppm (t, J = 2.2 Hz, CH_3); ^{19}F NMR (376 MHz, $CDCl_3$): δ = –146.74 ppm (q, J = 32.4 Hz); HR-APCI-TOF: m/z (%): 398.1860 (50) $[M+H]^+$ (calcd for $C_{21}H_{23}BF_2N_3O_2^+$: 398.1851), 378.1798 (100) $[M–F]^+$ (calcd for $C_{21}H_{22}BFN_3O_2^+$: 378.1789).

10-(3,5-dimethyl-4-nitrophenyl)-5,5-difluoro-2,8-diiodo-1,3,7,9-tetramethyl-5*H*-4λ^4,5λ^4-dipyrrolo[1,2-*c*:2',1'-*f*][1,3,2]diazaborinine (6).

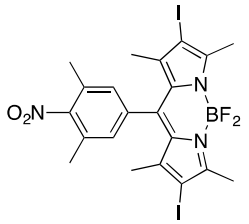

To a solution of **5** (9.54 g, 24.0 mmol, 1.00 equiv) in CH_2Cl_2 (1.60 L) was added *N*-iodosuccinimide (21.6 g, 96.1 mmol, 4.00 equiv). The resulting, bright pink, clear solution was stirred at rt for 12 h, then the solvent was removed in vacuo. Purification of the crude product mixture by FC (SiO_2; CH_2Cl_2/hexanes 1:2) yielded **6** (14.6 g, 22.5 mmol, 93%) as a pink, crystalline solid. R_f = 0.33 (SiO_2; CH_2Cl_2/hexanes 1:2); ^{1}H NMR (400 MHz, $CDCl_3$): δ = 7.09 (s, 2H, ArH), 2.65 (s, 6H, CH_3), 2.39 (s, 6H, CH_3), 1.46 ppm (s, 6H, CH_3); ^{13}C NMR (101 MHz, CD_2Cl_2): δ = 157.8, 153.0, 145.7, 139.5, 137.1, 132.0, 131.4, 129.1, 86.3, 17.9, 17.8, 16.5 ppm (t, J = 2.5 Hz, CH_3); ^{19}F NMR (376 MHz, $CDCl_3$): δ = –146.17 ppm (q, J = 33.8 Hz); HR-ESI-MS: m/z (%): 649.9773 (100, $[M+H]^+$, calcd for $C_{21}H_{21}BF_2I_2N_3O_2^+$: 649.9784).

4-(5,5-difluoro-2,8-diiodo-1,3,7,9-tetramethyl-5*H*-4λ^4,5λ^4-dipyrrolo[1,2-*c*:2',1'-*f*][1,3,2]diazaborinin-10-yl)-2,6-dimethylaniline (7).

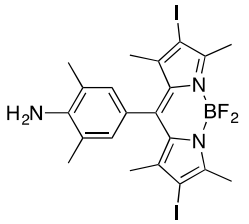

A round-bottomed flask was charged with a solution of nitro-BODIPY **6** (14.6 g, 22.4 mmol, 1.00 equiv) and $SnCl_2 \cdot 2H_2O$ (203 g, 897 mmol, 40.0 equiv) in methanol (883 mL), CH_2Cl_2 (883 mL), and 6 M HCl (283 mL). After stirring at rt for 8 h, the reaction mixture was diluted by addition of CH_2Cl_2 (300 mL, then successively washed with 2 M NaOH (3 x 1.00 L), water 3 x 1.00 L), and brine (1 x 1.00 L). The organic layer was dried over $MgSO_4$, filtered, and concentrated in vacuo. Purification of the crude product

mixture by FC (SiO_2; CH_2Cl_2/hexanes 1:2 → 1:1) afforded **7** (11.1 g, 17.9 mmol, 80%) as a magenta, crystalline solid. R_f = 0.25 (SiO_2, CH_2Cl_2/hexanes 1:2); ^{1}H NMR (400 MHz, $CDCl_3$): δ = 6.77 (s, 2H, ArH), 3.80 (s, 2H, NH_2), 2.63 (s, 6H, CH_3), 2.22 (s, 6H, CH_3), 1.48 ppm (s, 6H, CH_3); ^{13}C NMR (101 MHz, CD_2Cl_2): δ = 155.9, 145.8, 144.4, 143.7, 132.2, 128.9, 127.7, 123.3, 122.7, 85.0, 17.5, 17.4, 16.0 ppm (t, J = 2.0 Hz, CH_3); ^{19}F NMR (376 MHz, CD_2Cl_2): δ = –146.15 ppm (t, J = 33.8 Hz); HR-ESI-MS: m/z (%): 620.0033 (100) $[M+H]^+$ calcd for $C_{21}H_{23}BF_2I_2N_3^+$: 620.0041).

4-(5,5-difluoro-1,3,7,9-tetramethyl-2,8-bis(phenylethynyl)-5*H*-4λ^4,5λ^4-dipyrrolo[1,2-*c*:2',1'-*f*][1,3,2]diazaborinin-10-yl)-2,6-dimethylaniline (9a).

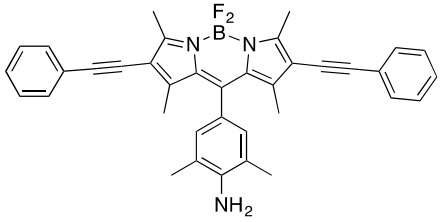

In an oven-dried Schlenk flask, a solution of diiodo-BODIPY **7** (7.27g, 11.7 mmol, 1.00 equiv) and phenylacetylene (5.14 mL, 46.8 mmol, 4.00 equiv) in triethylamine (358 mL) and THF (1.10 L) was de-gassed by bubbling N_2 through the solution for 15 min. [$(PPh_3)_2PdCl_2$] (821 mg, 1.17 mmol, 0.10 equiv) and CuI (446 mg, 2.34 mmol, 0.20 equiv) were added to the solution, and the resulting mixture was stirred for 12 h at 65 °C under an atmosphere of N_2. After removing the solvents in vacuo, the crude product mixture was purified by FC (SiO_2; CH_2Cl_2/hexanes 1:1) to yield **9a** (5.33 g, 9.39 mmol, 80%) as an iridescent, pink, crystalline solid. R_f = 0.33 (SiO_2, CH_2Cl_2/hexanes 1:1); ^{1}H NMR (400 MHz, $CDCl_3$): δ = 7.47 –7.45 (m, 4H, ArH), 7.35 – 7.34 (m, 6H, ArH), 6.83 (s, 2H, ArH), 3.82 (s, 2H, NH_2), 2.71 (s, 6H, CH_3), 2.24 (s, 6H, CH_3), 1.63 ppm (s, 6H, CH_3); ^{13}C NMR (125 MHz, CD_2Cl_2): δ = 157.7, 144.9, 144.6, 144.4, 132.1, 131.4, 128.6, 128.3, 127.8, 123.7, 123.0, 122.6, 115.8, 96.4, 82.0, 17.6, 13.9, 13.6 (br s, CH_3) ppm; ^{19}F NMR (376 MHz, CD_2Cl_2): δ = –146.79 ppm (q, J = 33.8 Hz); HR-MALDI-MS (DTL): m/z (%): 548.2651 (100) $[M–F]^+$ (calcd for $C_{37}H_{32}BFN_3^+$: 548.2673), 567.2685 (37) $[M]^+$, calcd for $C_{37}H_{32}BF_2N_3^+$: 567.2657).

4-(2,8-bis((9-ethyl-9*H*-carbazol-3-yl)ethynyl)-5,5-difluoro-1,3,7,9-tetramethyl-5*H*-4λ^4,5λ^4-dipyrrolo[1,2-*c*:2',1'-*f*][1,3,2]diazaborinin-10-yl)-2,6-dimethylaniline (9b).

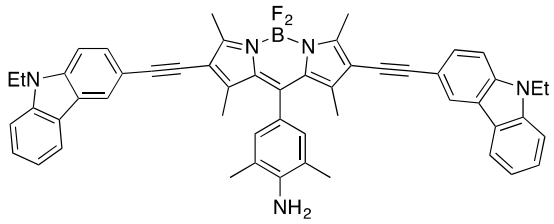

In an oven-dried Schlenk flask, a solution of diiodo-BODIPY **7** (1.17, 11.7 mmol, 1.00 equiv) and carbazoyl alkyne **8b** (1.66 g, 7.57 mmol, 4.00 equiv) in triethylamine (58.0 mL) and THF (175 mL) was de-gassed by bubbling N_2 through the solution for 15 min. [$(PPh_3)_2PdCl_2$] (133 mg, 189 μmol, 0.10 equiv) and CuI (72.0 mg, 378 μmol, 0.20 equiv) were added to the solution, and the resulting brown mixture was stirred for 12 h at 65 °C under an atmosphere of N_2. After removing the solvents in vacuo, the crude product mixture was purified by FC (SiO_2; CH_2Cl_2/hexanes 1:1 → 2:1) to yield **9b** (1.10 g, 1.37 mmol, 73%) as an iridescent, blue, crystalline solid. R_f = 0.40 (SiO_2, CH_2Cl_2/hexanes 1:1); ^{1}H NMR (400 MHz, CD_2Cl_2): δ = 8.23 (s, 2H, ArH), 8.09 (d, J = 9.4 Hz, 2H, ArH), 7.59 (d, J = 9.9 Hz, 2H, ArH), 7.54 – 7.37 (m, 6H, ArH), 7.25 (t, J = 8.0 Hz, 2H, ArH), 6.89 (s, 2H, ArH), 4.38 (q, J = 7.4 Hz, 4H, NCH_2CH$_3$), 3.87 (br s, 2H, NH_2), 2.74 (s, 6H, CH_3), 2.26 (s, 6H, CH_3), 1.43 ppm (t, J = 7.1 Hz, 6H, NCH$_2$CH_3); ^{13}C NMR (101 MHz, CD_2Cl_2): δ = 157.5, 144.3, 143.8, 140.6, 139.7, 129.1, 127.9, 126.4, 123.7, 123.2, 123.1, 122.6, 122.5, 120.7, 119.5, 113.6, 109.0, 108.9, 97.7, 79.9, 37.9, 17.6, 13.9, 13.8, 13.7 ppm (br t, J = 2.0 Hz, CH_3), 3 carbons not found; ^{19}F NMR (376 MHz, CD_2Cl_2): δ = –146.84 ppm (q, J = 33.8 Hz); HR-MALDI-MS (DTL): *m*/*z* (%): 782.3865 (92) [M–F]$^+$ (calcd for $C_{53}H_{46}BFN_5^+$: 782.3830), 801.3837 (100) [M]$^+$ (calcd for $C_{53}H_{46}BF_2N_5^+$: 801.3814).

2,3-dichloro-6-(4-(5,5-difluoro-1,3,7,9-tetramethyl-2,8-bis(phenylethynyl)-5*H*-4λ^4,5λ^4-dipyrrolo[1,2-*c*:2',1'-*f*][1,3,2]diazaborinin-10-yl)-2,6-dimethylphenyl)-5*H*-pyrrolo[3,4-*b*]pyrazine-5,7(6*H*)-dione (2a).

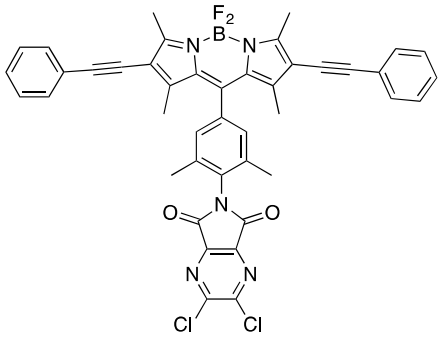

An oven-dried Schlenk flask was charged with a mixture of **9a** (4.70 g, 8.92 mmol, 1.00 equiv) and anhydride **10** (1.90 g, 11.6 mmol, 1.30 equiv) in THF (125 mL). The mixture was heated to 60 °C and

stirred for 12 h under an atmosphere of N_2, at which point, consumption of **9a** was observed by TLC. The reaction mixture was allowed to cool to room temperature before sequential, dropwise addition of pyridine (2.38 mL, 29.4 mmol, 3.30 equiv) and oxalyl chloride (1.15 mL, 13.4 mmol, 1.50 equiv). After the mixture ceased bubbling, it was heated to 50 °C and stirred for 12 h. The mixture was cooled to rt, the solvent was removed in vacuo, and the insoluble residue was dry loaded onto SiO_2 for purification by FC (SiO_2, CH_2Cl_2) to afford **2a** (4.38 g, 5.35 mmol, 60%) as a pink, iridescent solid. $R_f = 0.40$ (SiO_2, CH_2Cl_2/hexanes 2:1); ^{1}H NMR (500 MHz, $CDCl_3$, 323 K): $\delta = 7.48 – 7.46$ (m, 4H, ArH), 7.33 – 7.32 (m, 6H, ArH), 7.22 (s, 2H, ArH), 2.74 (s, 3H, CH_3), 2.24 (s, 3H, CH_3), 1.70 ppm (s, 3H, CH_3); ^{13}C NMR not obtained due to poor solubility; ^{19}F NMR (376 MHz, $CDCl_3$, 303 K): $\delta = –146.80$ ppm (q, $J = 30.0$ Hz); UV/Vis (CH_2Cl_2): λ_{max} (ε) = 304 (28000), 406 (11000), 540 (sh), 576 (52000) nm; HR-MALDI-MS (DTL): *m*/*z* (%): 767.1836 (59) $[M]^+$ (calcd for $C_{43}H_{30}BCl_2F_2N_5O_2^+$: 767.1838), 748.1856 (100) $[M–F]^+$ (calcd for $C_{43}H_{30}BCl_2FN_5O_2^+$: 748.1854).

6-(4-(2,8-bis((9-ethyl-9*H*-carbazol-3-yl)ethynyl)-5,5-difluoro-1,3,7,9-tetramethyl-5*H*-4λ^4,5λ^4-dipyrrolo[1,2-*c*:2',1'-*f*][1,3,2]diazaborinin-10-yl)-2,6-dimethylphenyl)-2,3-dichloro-5*H*-pyrrolo[3,4-*b*]pyrazine-5,7(6*H*)-dione (2b).

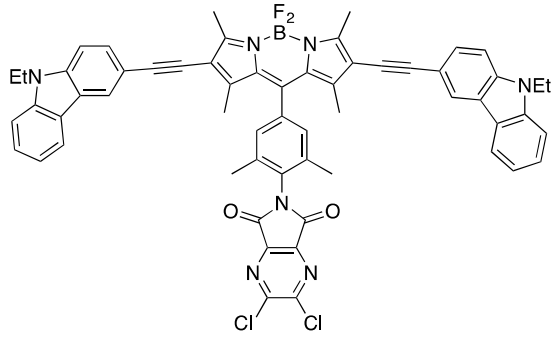

An oven-dried Schlenk flask was charged with a mixture of **9b** (1.05 g, 1.31 mmol, 1.00 equiv) and anhydride **10** (374 mg, 1.71 mmol, 1.30 equiv) in THF (25 mL). The mixture was heated to 60 °C and stirred for 12 h under an atmosphere of N_2, at which point, consumption of **9b** was observed by TLC. The reaction mixture was allowed to cool to room temperature before sequential, dropwise addition of pyridine (350 μL, 4.32 mmol, 3.30 equiv) and oxalyl chloride (170 μL, 1.97 mmol, 1.50 equiv). After the mixture ceased bubbling, it was heated to 50 °C and stirred for 12 h. The mixture was cooled to rt, the solvent was removed in vacuo, and the insoluble residue was dry loaded onto SiO_2 for purification by FC (SiO_2, MeOH/CH_2Cl_2 1:9) to afford **2b** (883 mg, 838 μmol, 64%) as a blue, iridescent solid. $R_f = 0.35$ (SiO_2, CH_2Cl_2/hexanes 2:1); ^{1}H NMR (500 MHz, d_6-DMSO, 323 K): $\delta = 8.42 – 8.33$ (m, 2H, ArH), 8.22 (d, $J = 8.4$ Hz, 2H, ArH), 7.69 – 7.55 (m, 6H, ArH), 7.51 – 7.48 (m, 2H, ArH), 7.39 (s, 2H, ArH), 7.29 – 7.17 (m, 2H, ArH), 4.46 (q, $J = 7.3$ Hz, 4H, NCH_2CH$_3$), 2.72 (s, 6H, CH_3), 2.23 (s, 6H, CH_3), 1.70 – 1.68

(m, 6H, CH_3), 1.34 ppm (t, J = 7.1 Hz, 6H, NCH_2CH_3); ^{13}C NMR not obtained due to poor solubility; ^{19}F NMR (376 MHz, CD_2Cl_2): δ = –146.90 ppm (q, J = 30.0 Hz); UV/Vis (CH_2Cl_2): λ_{max} (ε) = 284 (47000), 305 (56000), 320 (sh), 351 (sh), 367 (sh), 425 (12000), 602 (42000) nm; HR-MALDI-MS (DTL): *m*/*z* (%): 1001.2969 (45) $[M]^+$ (calcd for $C_{59}H_{44}BCl_2F_2N_7O_2^+$: 1001.2995), 982.3023 (100) $[M–F]^+$ (calcd for $C_{59}H_{44}BCl_2FN_7O_2^+$: 982.3011).

Cavitand (1).

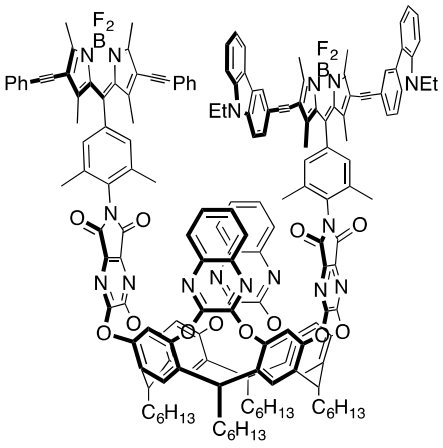

A flame-dried Schlenk flask was charged with a mixture of phenyl wall **2a** (28.5 mg, 37.0 μmol, 1.00 equiv), carbazole arm **2b** (37.2 mg, 37.0 µmol, 1.00 equiv), and tetrol **11** (40.0 mg, 37.0 µmol, 1.00 equiv) in THF (15 mL). The mixture was warmed to 50 °C and Cs_2CO_3 (50.8 mg, 156 µmol, 4.20 equiv) was added. The mixture was stirred at 50 °C for 4 h, then allowed to cool to room temperature and filtered over silica. The eluent was concentrated in vacuo, and the resulting residue was flash chromatographed (SiO_2, CH_2Cl_2) to yield an impure fraction (R_f = 0.50) containing the desired product. The impure product mixture was subjected to recycling gel permeation chromatography (Jaigel H1 + Jaigel H2 columns in sequence, each 20 mm ID x 300 mm length; $CHCl_3$, 4 mL min^{-1}) to afford 1 (27 mg, 10 µmol, 17%) as a dark blue solid. R_f = 0.50 (SiO_2, CH_2Cl_2); t_R = 32.6 min; ^{1}H NMR (500 MHz, $CDCl_3$, 323 K): δ = 8.32–8.30 (m, 4H), 8.10 (br s, 2H), 8.05 – 7.95 (m, 6H, ArH), 7.47 – 7.26 (m, 22H, ArH), 7.25 – 7.13 (m, 10H, ArH), 5.78 (t, J = 7.9 Hz, 2H, $C_6H_{13}CHAr_2$), 5.68 (br m, 2H, $C_6H_{13}CHAr_2$), 4.26 (q, J = 7.4 Hz, 4H, NCH_2CH_3), 2.74 – 2.67 (m, 10H), 2.36 – 2.25 (m, 14H), 1.70 – 1.67 (m, 10H), 1.50 – 1.22 (m, 48H), 0.98 – 0.94 ppm (m, 12H); ^{13}C NMR (126 MHz, CDCl3, 303 K): δ = ^{13}C NMR (126 MHz, $CDCl_3$) δ 161.3, 159.1, 153.3, 152.6, 152.4, 152.3, 143.6, 141.8, 140.6, 140.1, 139.6, 137.1, 136.0, 131.1, 129.9, 129.8, 129.5, 129.0, 128.3, 128.1, 126.2, 124.0, 123.8, 123.3, 123.2, 122.7, 120.9, 119.5, 119.1, 113.6, 109.0, 108.4, 98.3, 96.9, 95.8, 81.8, 37.8, 34.6, 34.5, 32.9, 32.4, 32.2, 30.4, 30.0, 29.7, 29.6, 28.3, 28.2, 23.0, 18.5, 14.4, 14.1, 14.0, 13.7 ppm; ^{19}F NMR (470 MHz, $CDCl_3$, 223 K): δ = –146.89 –

147.02 ppm (br m); UV/Vis ($CHCl_3$): λ_{max} (ε) = 305 (126000), 320 (sh), 369 (sh), 422 (31000), 576 (122000), 620 (sh) nm; HR-ESI-MS (MeOH/CH_2Cl_2 1:1): *m/z* (%): 2702.1402 (38) [*M*]+ (calcd for $C_{170}H_{146}B_2F_4N_{16}O_{12}^+$: 2702.1462), 1351.0708 (100) $[M]^{2+}$ (calcd for $C_{170}H_{146}B_2F_4N_{16}O_{12}^{2+}$: 1351.0731).

S2. ^{1}H, ^{13}C, and ^{19}F NMR Spectra of Prepared Compounds

S2.1. Characterization Spectra of Prepared Compounds

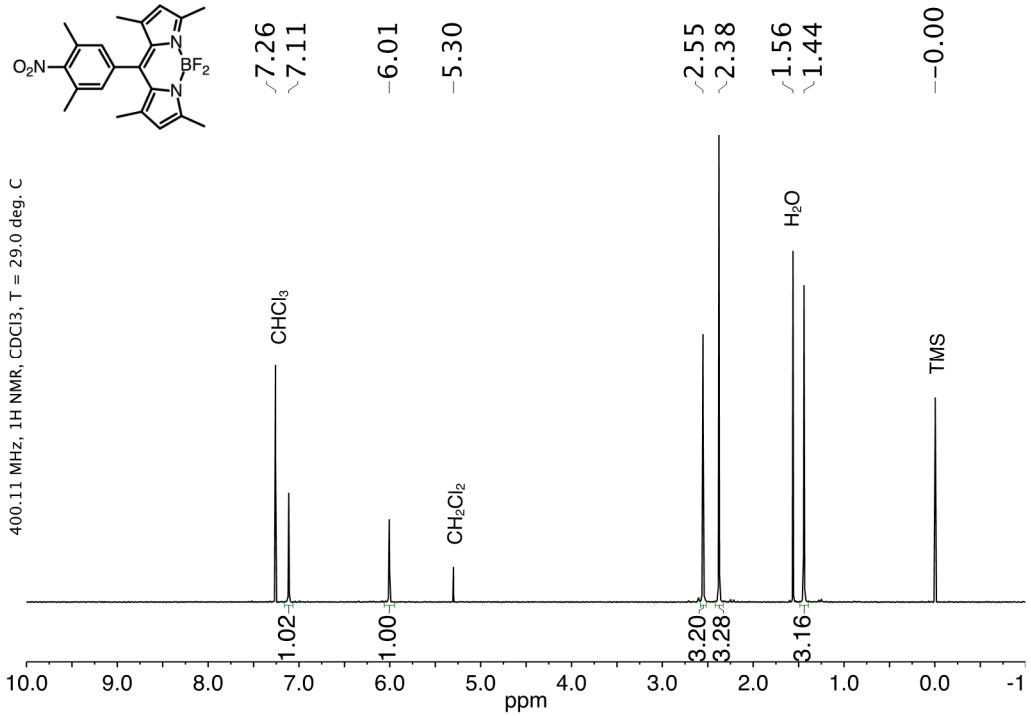

Figure S1. ^{1}H NMR spectrum (400 MHz) of nitro-BODIPY **5**.

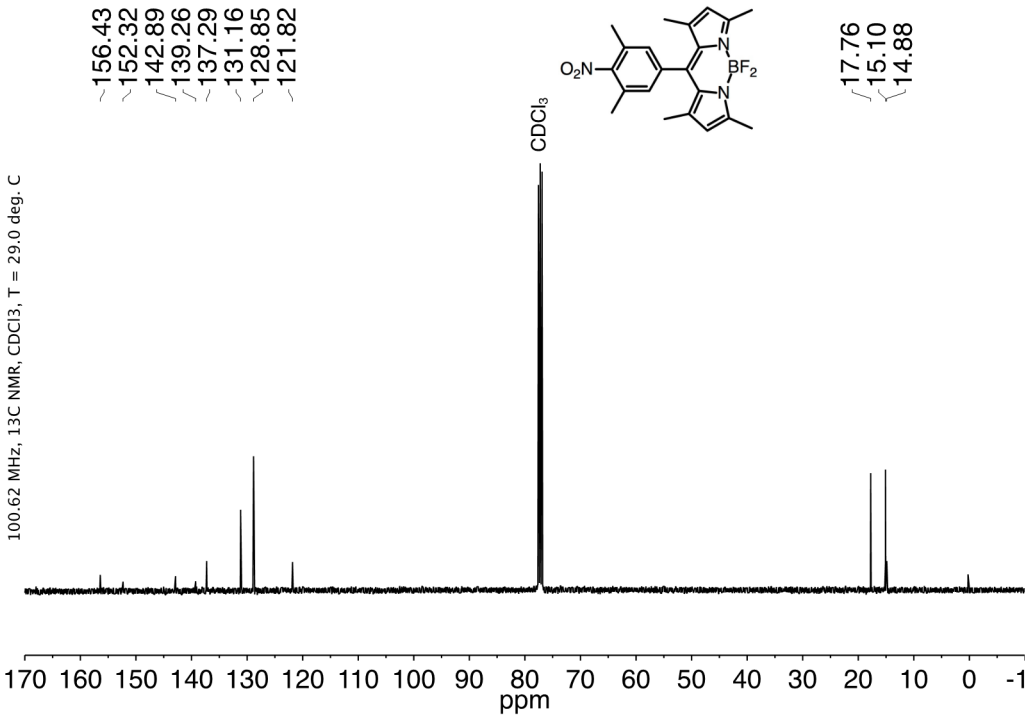

Figure S2. ^{13}C NMR spectrum (101 MHz) of nitro-BODIPY **5**.

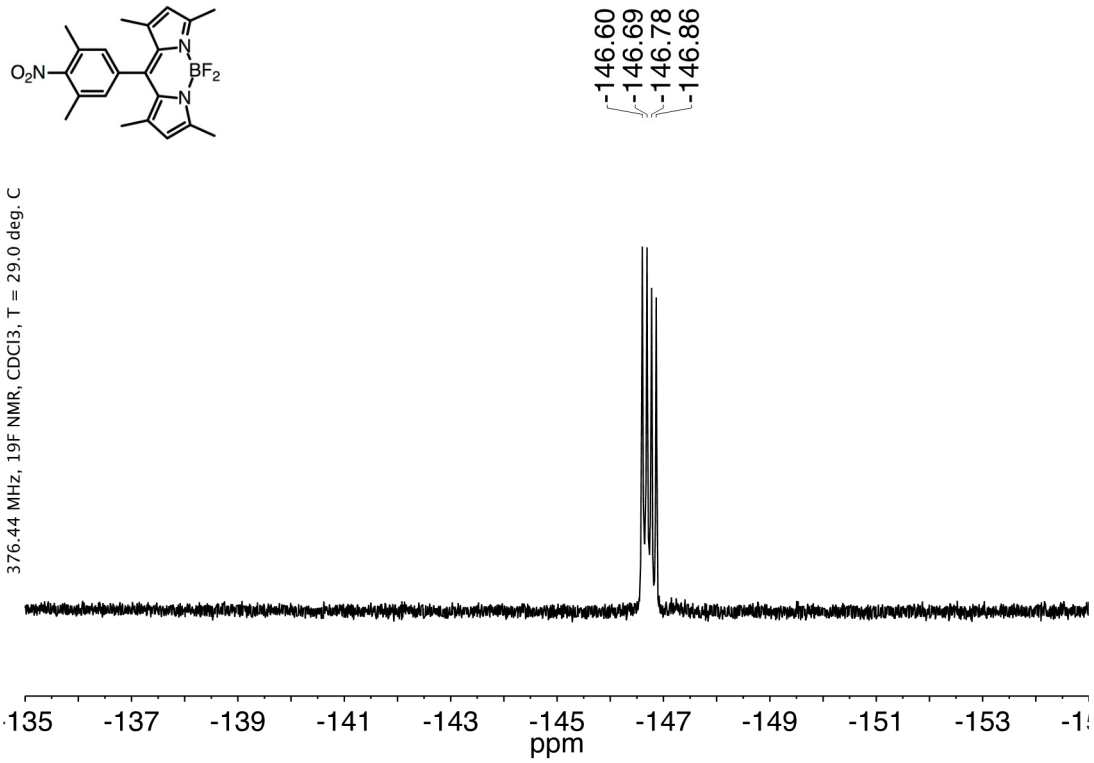

Figure S3. ^{19}F NMR spectrum (376 MHz) of nitro-BODIPY **5**.

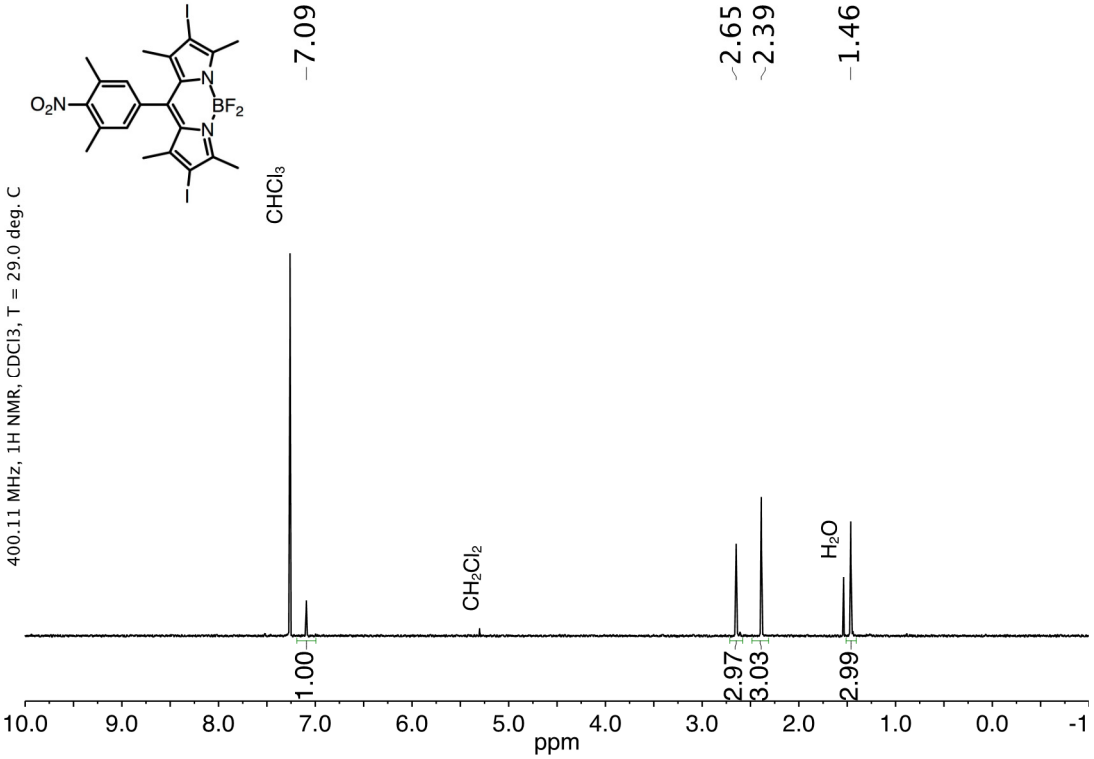

Figure S4. ^{1}H NMR spectrum (400 MHz) of diiodo-BODIPY **6**.

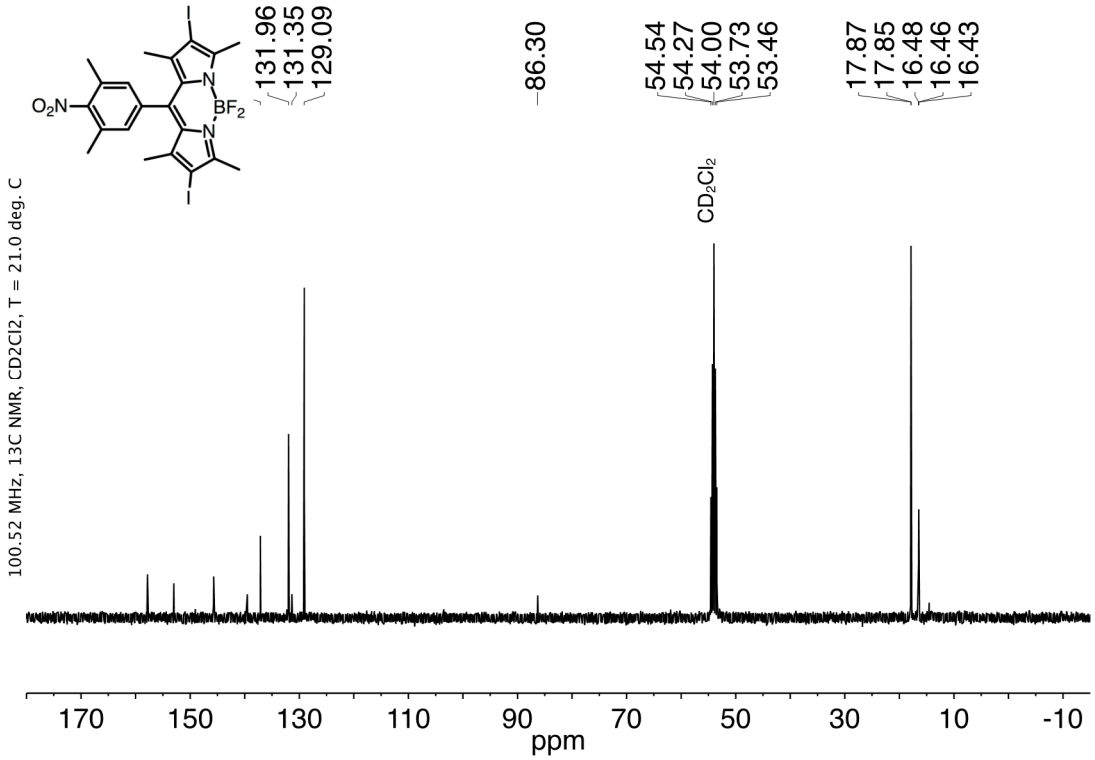

Figure S5. ^{13}C NMR spectrum (101 MHz) of diiodo-BODIPY **6**.

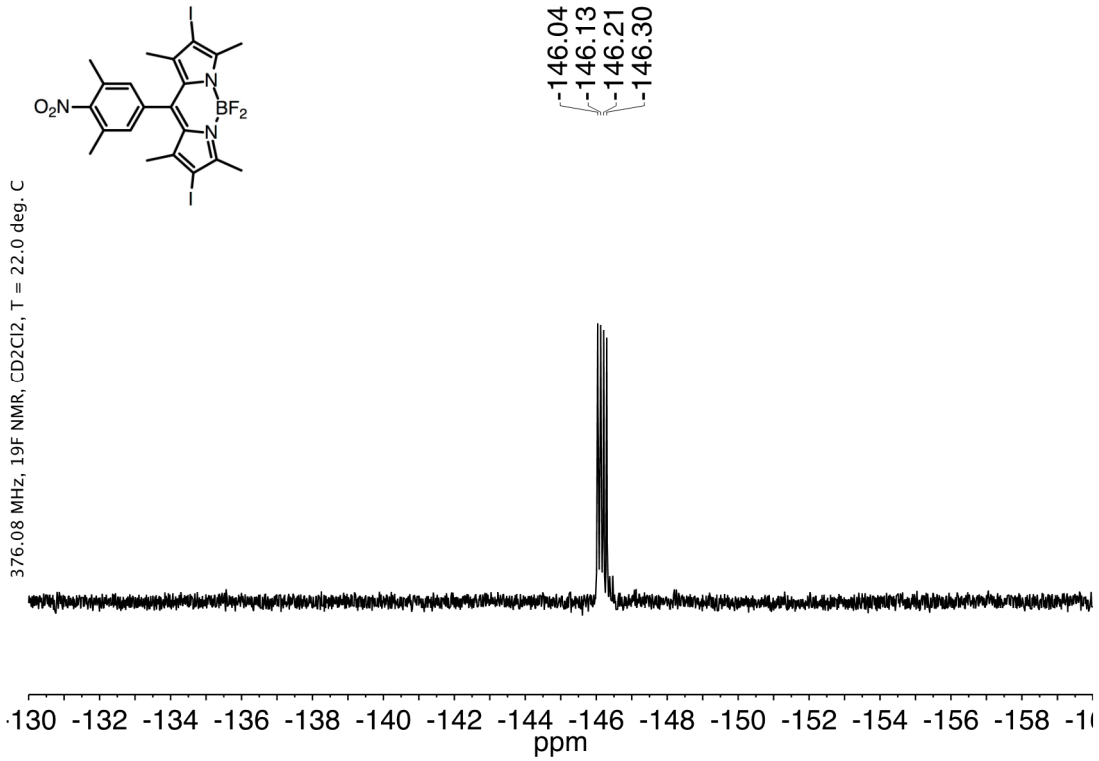

Figure S6. ^{19}F NMR spectrum (376 MHz) of diiodo-BODIPY **6**.

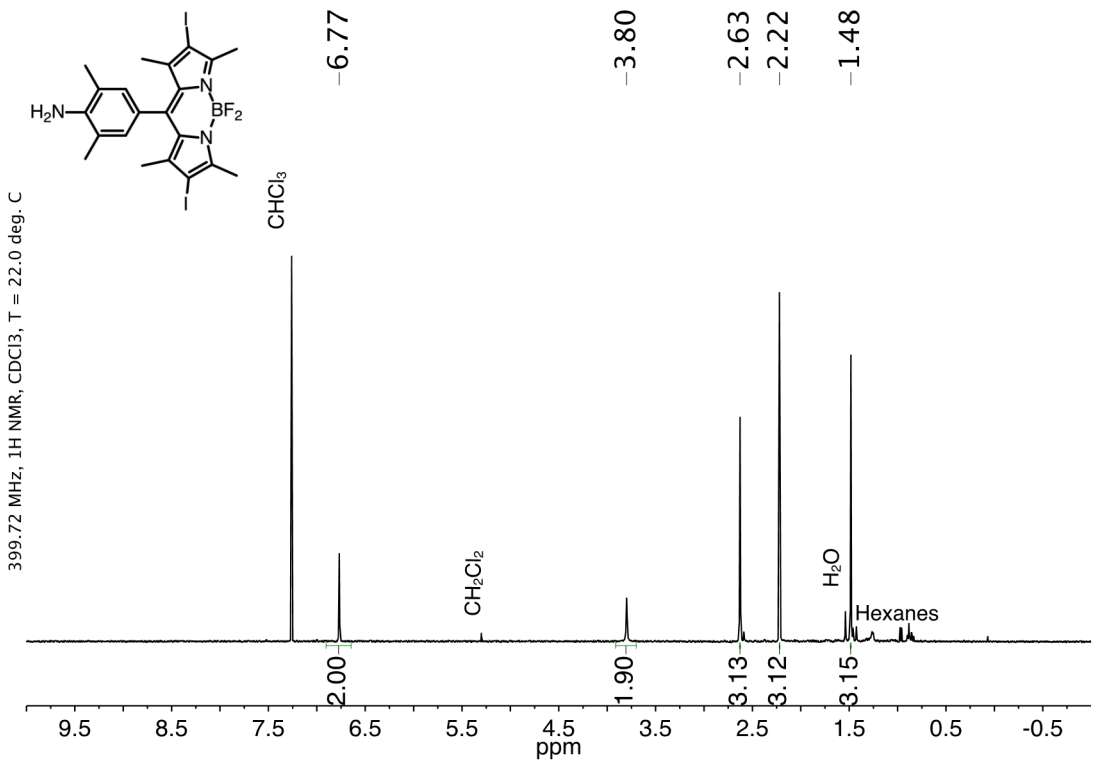

Figure S7. [1]H NMR spectrum (400 MHz) of anilino-BODIPY **7**.

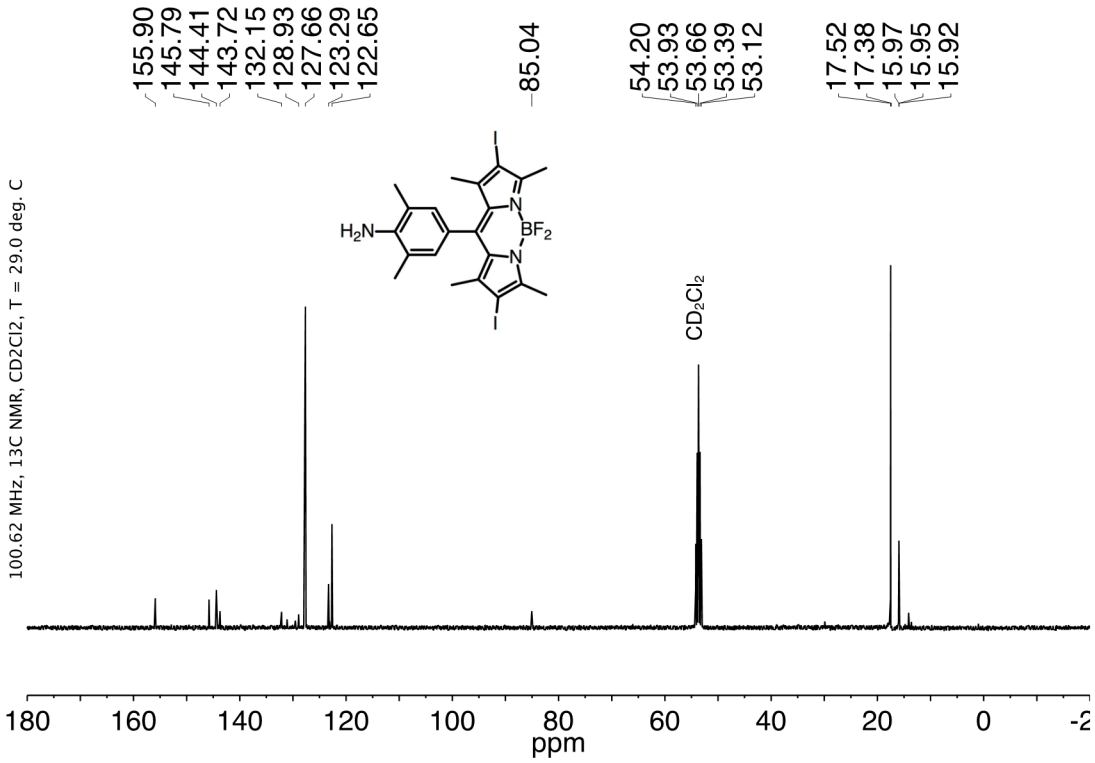

Figure S8. [13]C NMR spectrum (101 MHz) of anilino-BODIPY **7**.

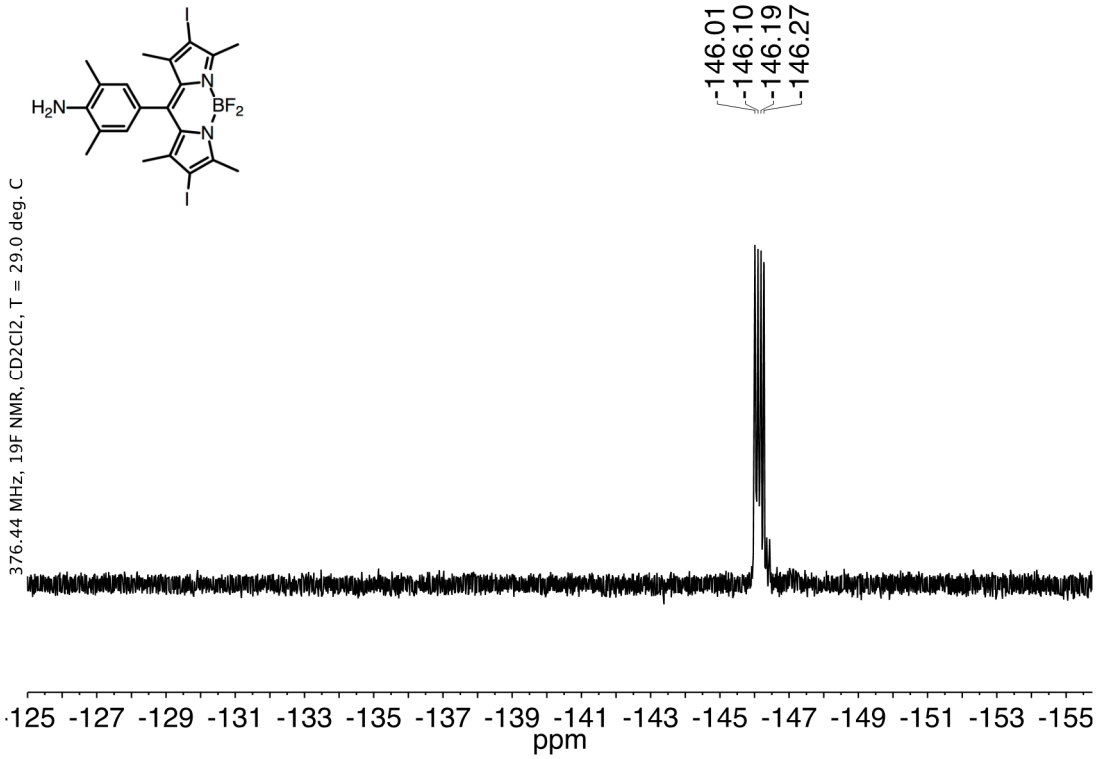

Figure S9. ^{19}F NMR spectrum (376 MHz) of anilino-BODIPY **7**.

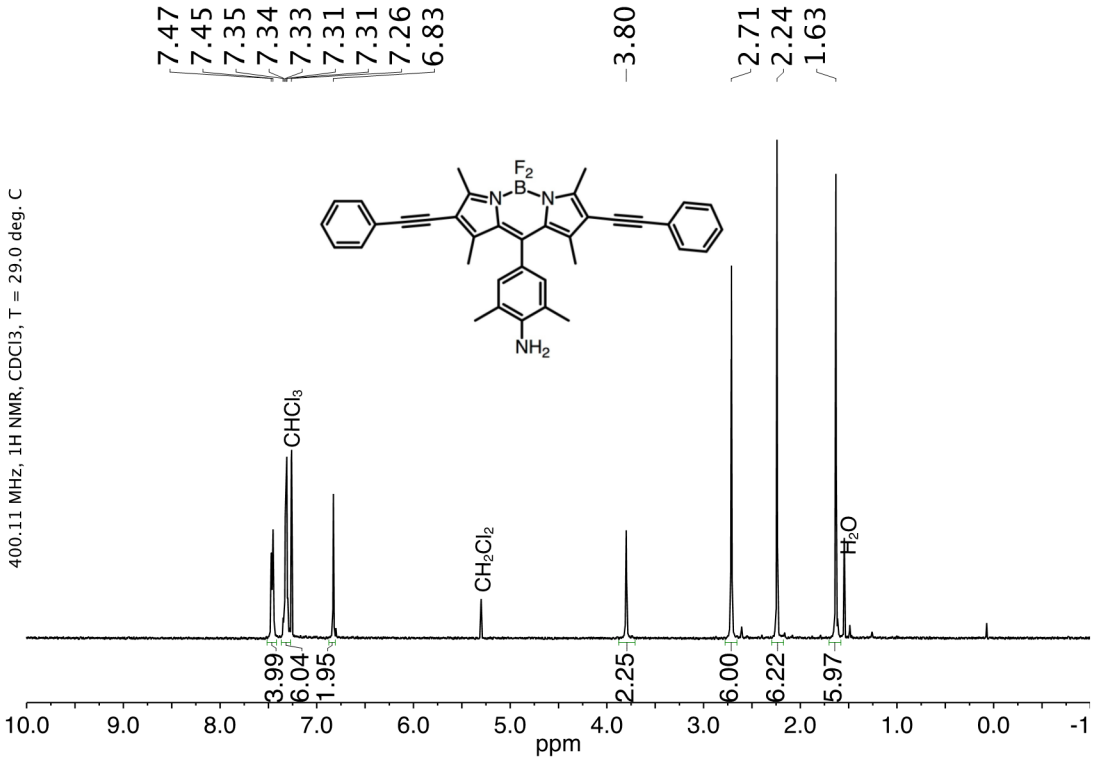

Figure S10. ^{1}H NMR spectrum (400 MHz) of donor dye **9a**.

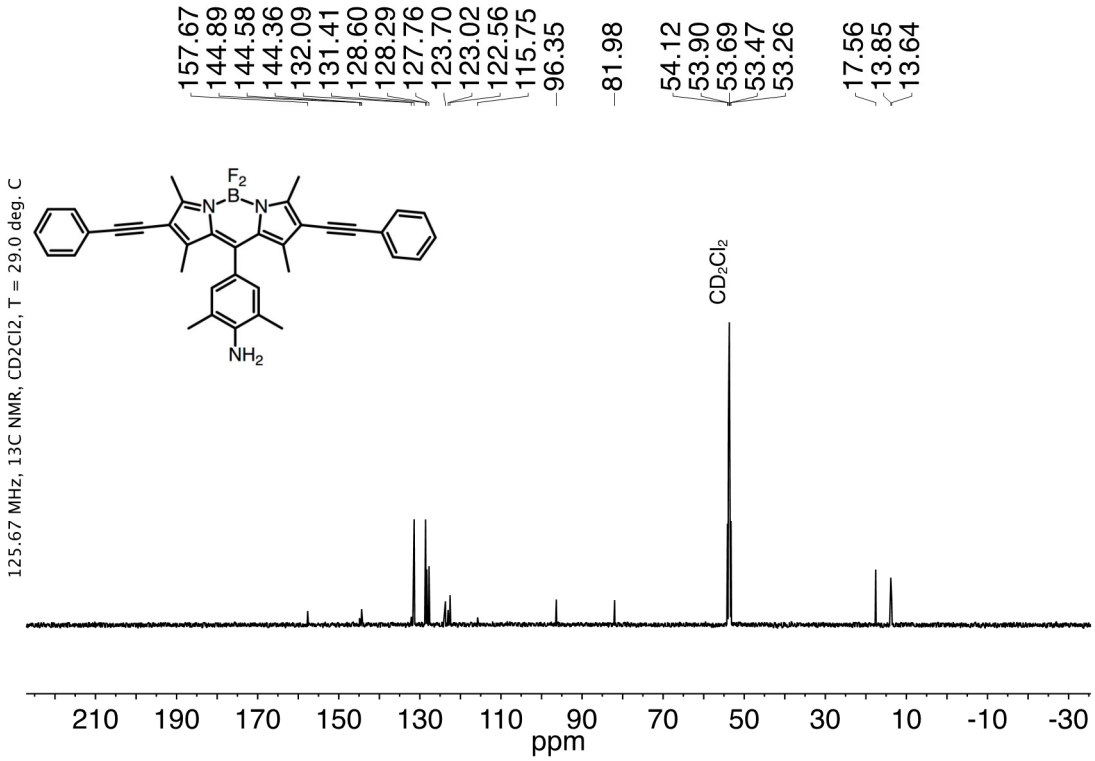

Figure S11. ^{13}C NMR spectrum (126 MHz) of donor dye **9a**.

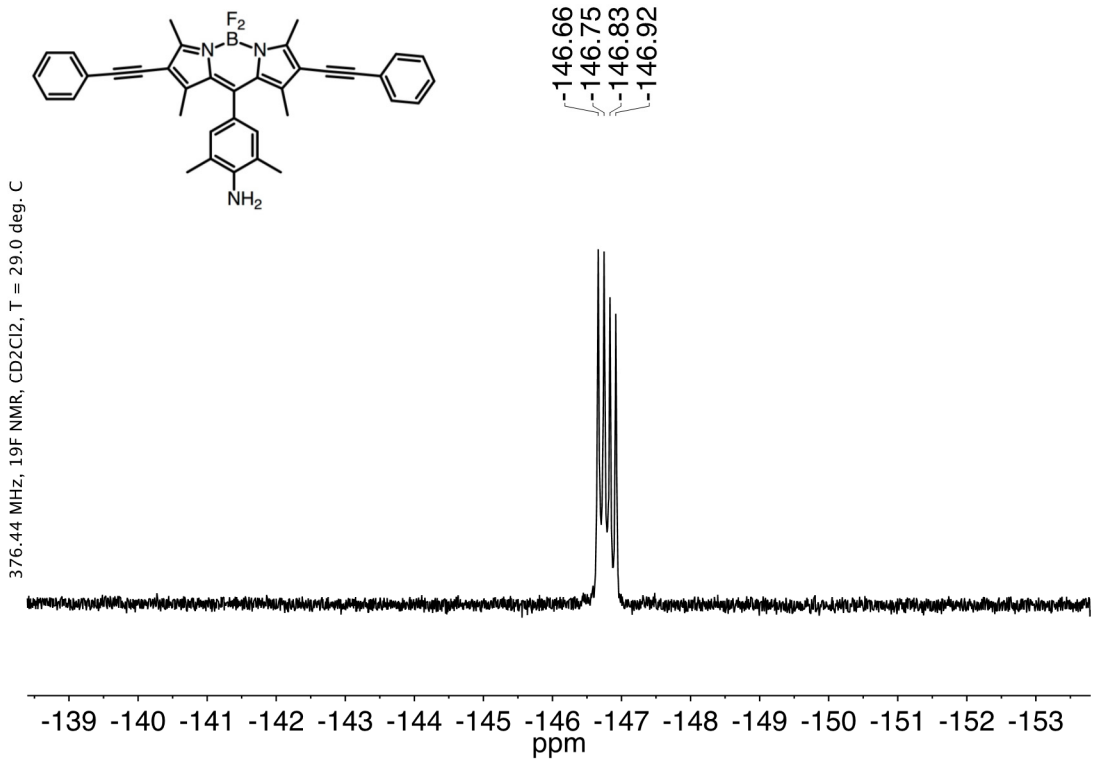

Figure S12. ^{19}F NMR spectrum (376 MHz) of donor dye **9a**.

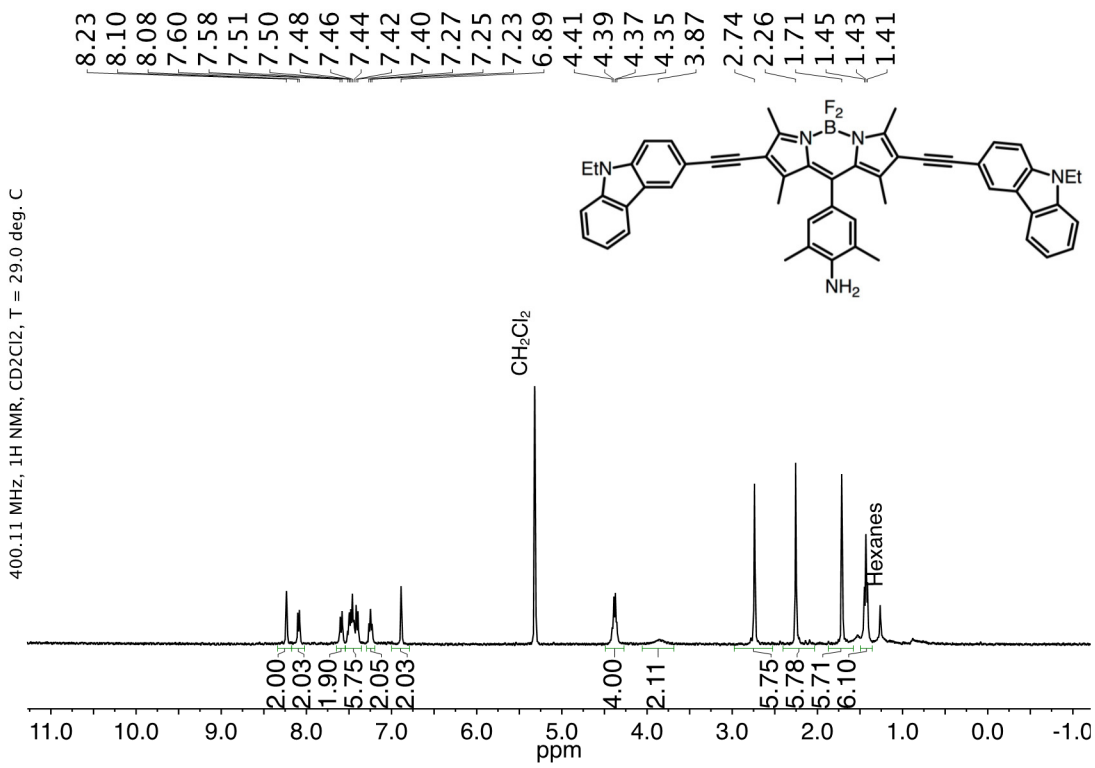

Figure S13. [1]H NMR spectrum (400 MHz) of acceptor dye **9b**.

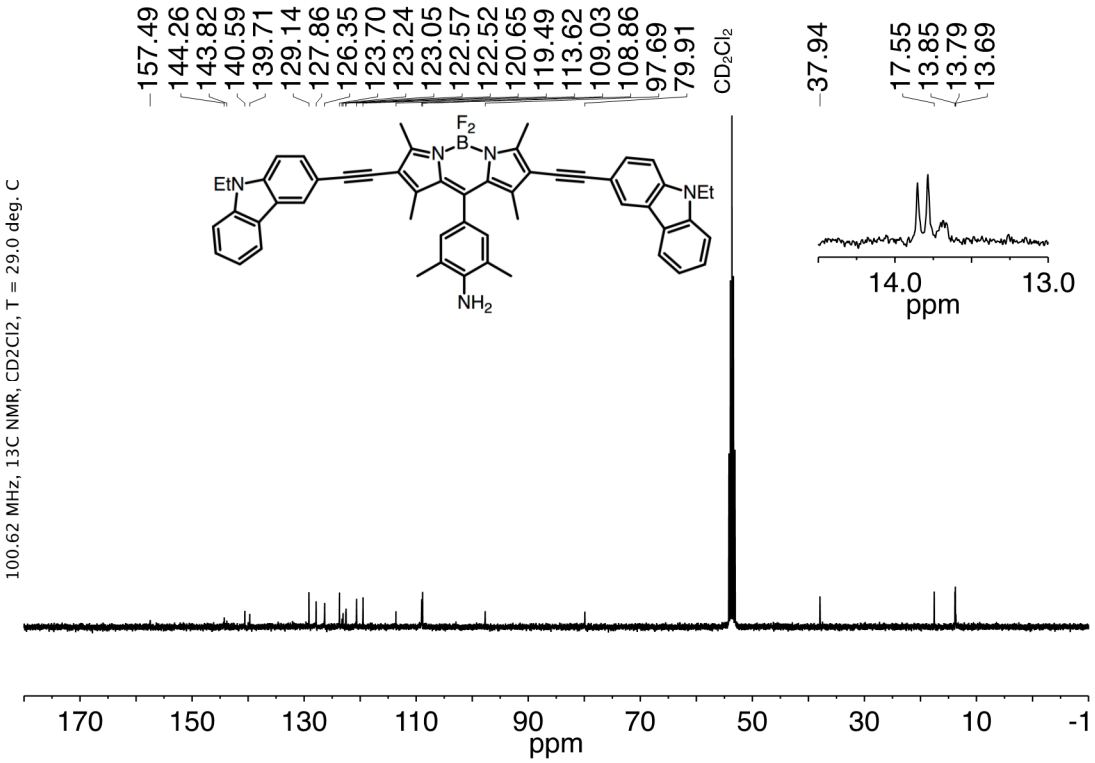

Figure S14. [13]C NMR spectrum (101 MHz) of acceptor dye **9b**.

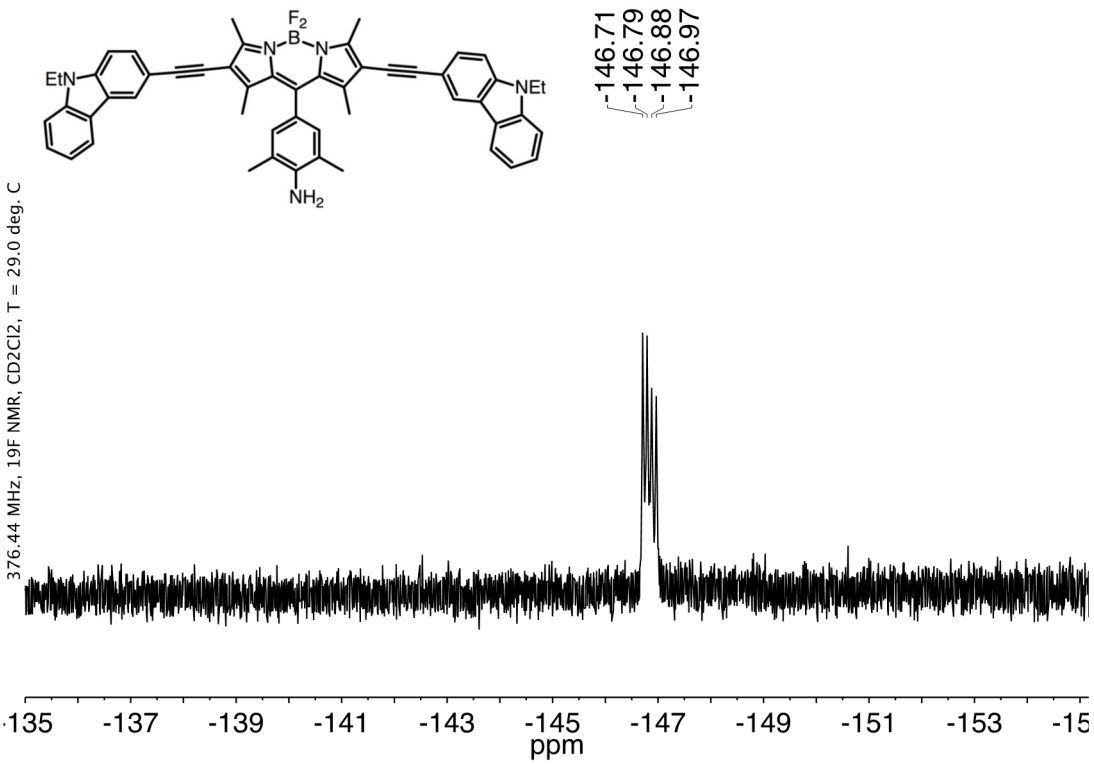

Figure S15. ^{19}F NMR spectrum (376 MHz) of acceptor dye **9b**.

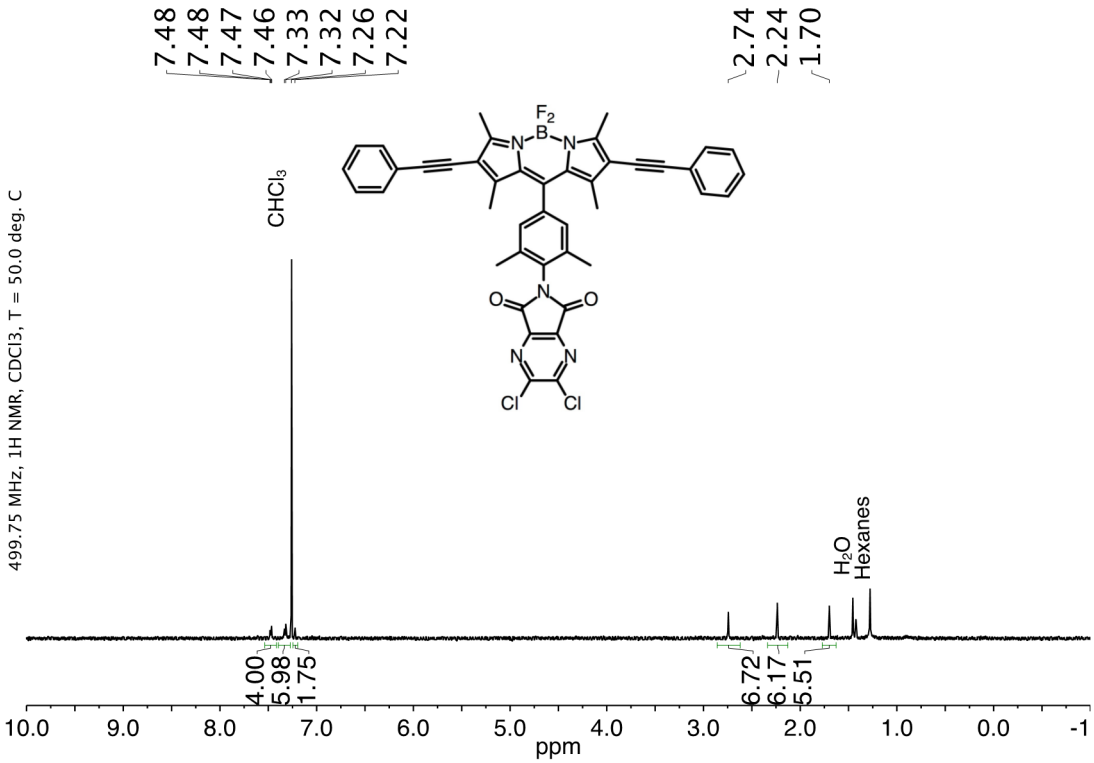

Figure S16. ^{1}H NMR spectrum (500 MHz) of donor flap **2a**.

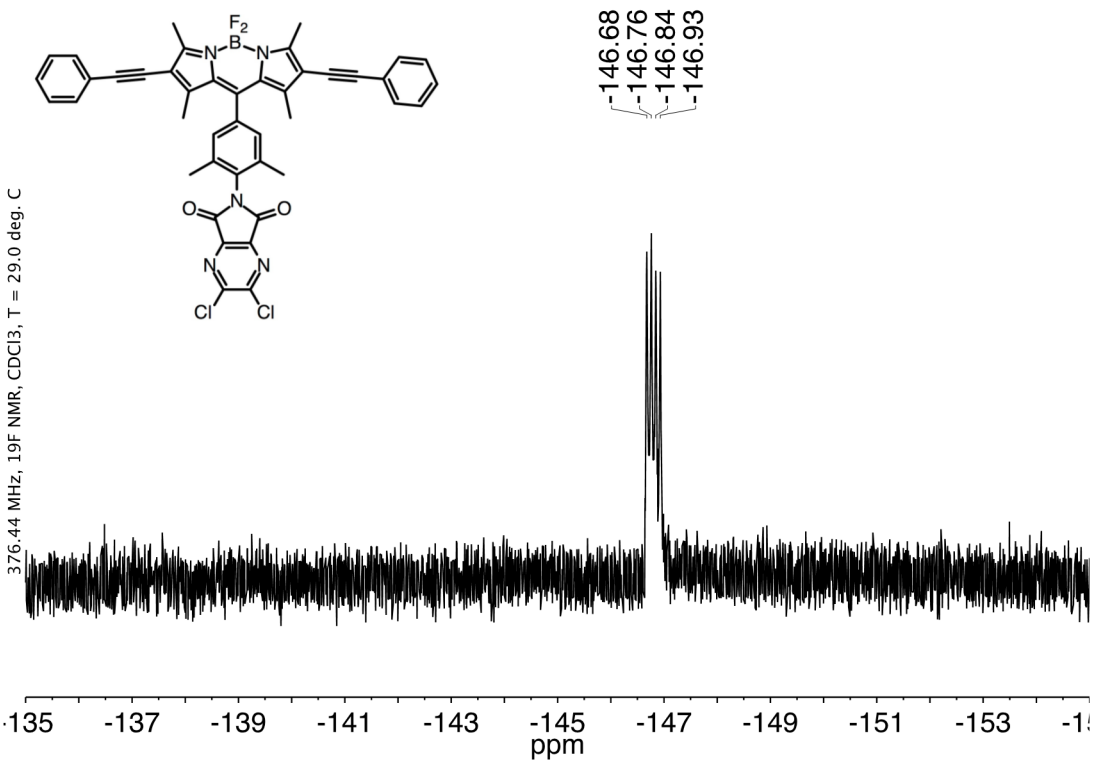

Figure S17. ^{19}F NMR spectrum (376 MHz) of donor flap **2a**.

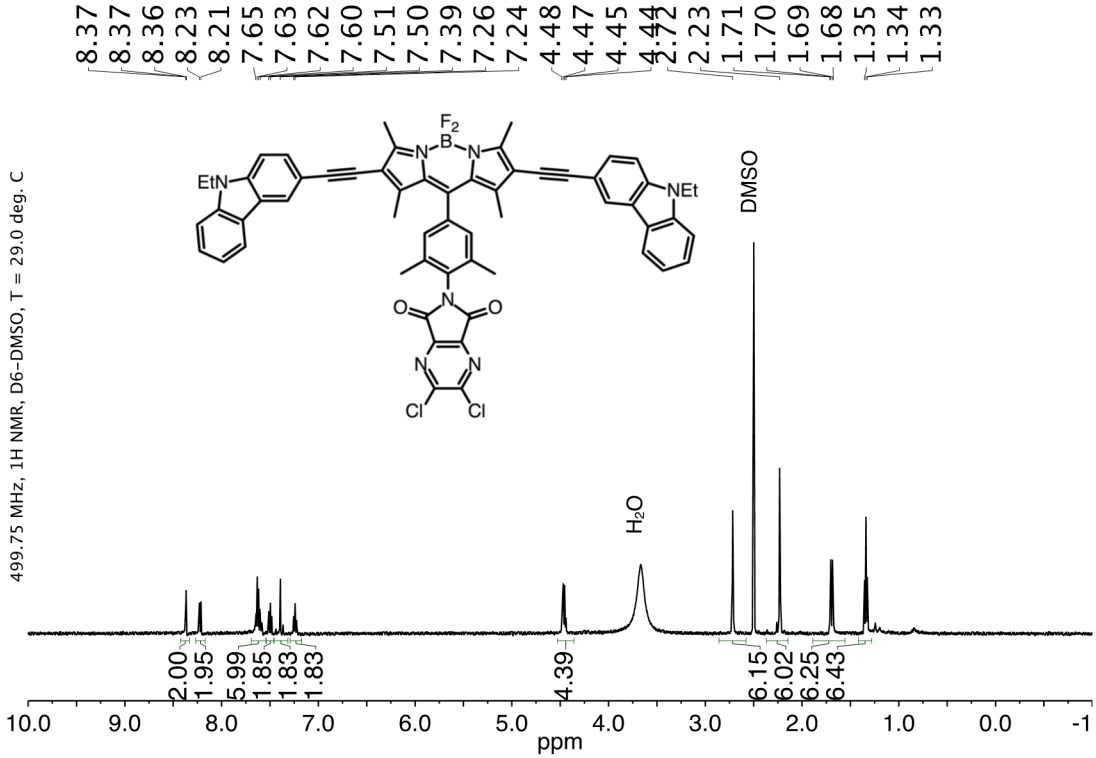

Figure S18. ^{1}H NMR spectrum (500 MHz) of acceptor flap **2b**.

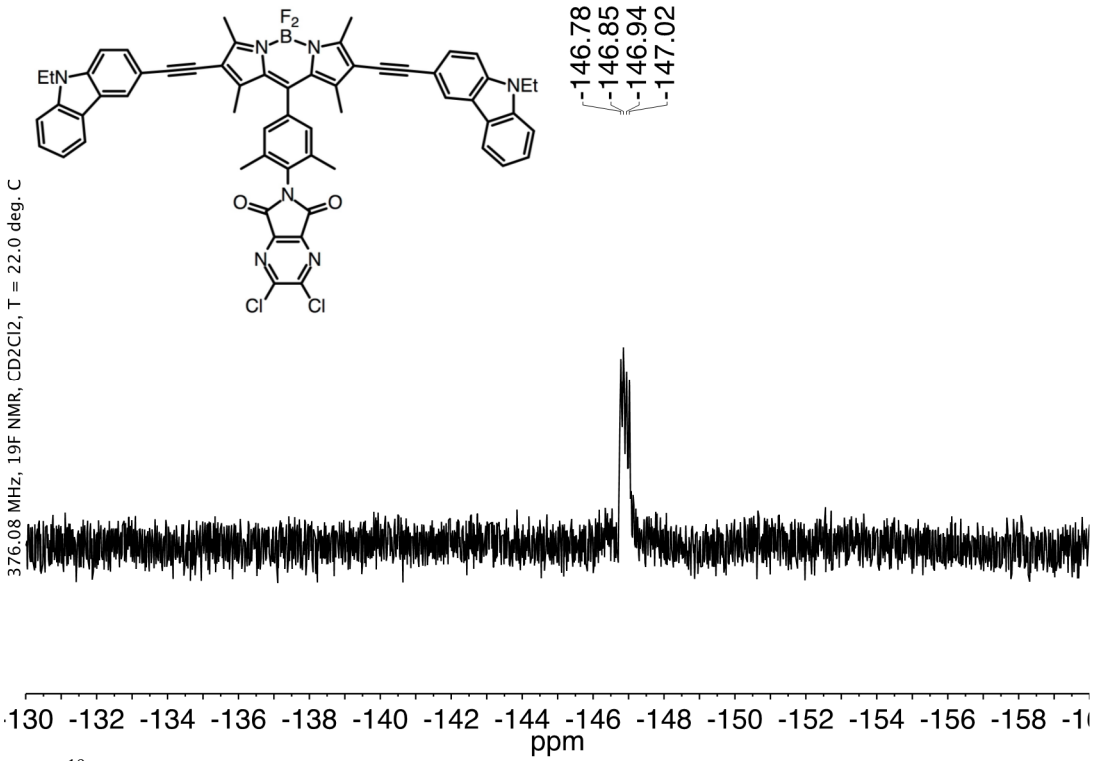

Figure S19. ^{19}F NMR spectrum (376 MHz) of acceptor flap **2b**.

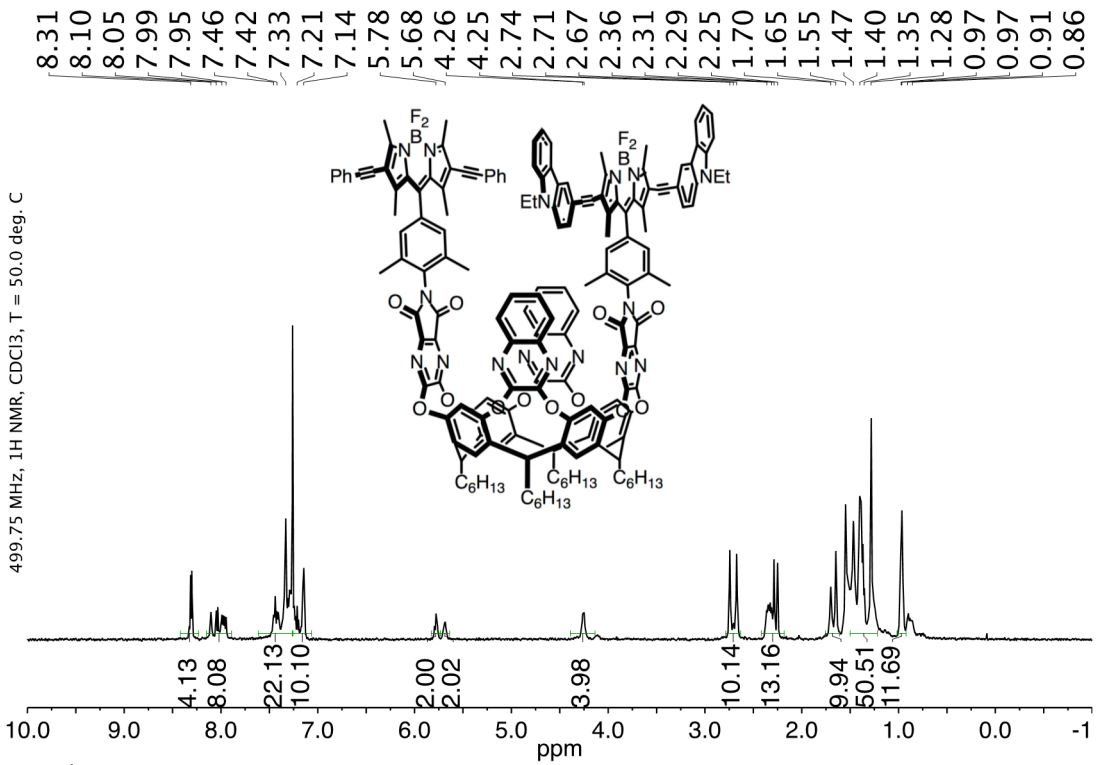

Figure S20. ^{1}H NMR spectrum (500 MHz) of cavitand **1**.

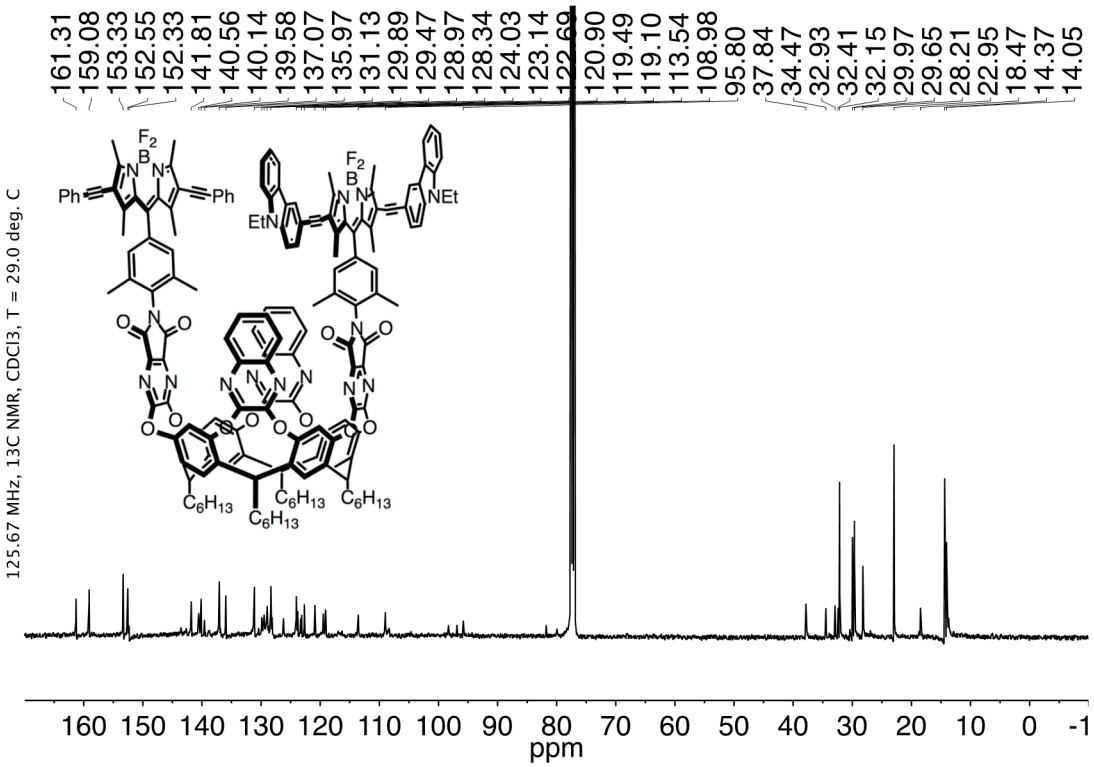

Figure S21. ^{13}C NMR spectrum (126 MHz) of cavitand **1**.

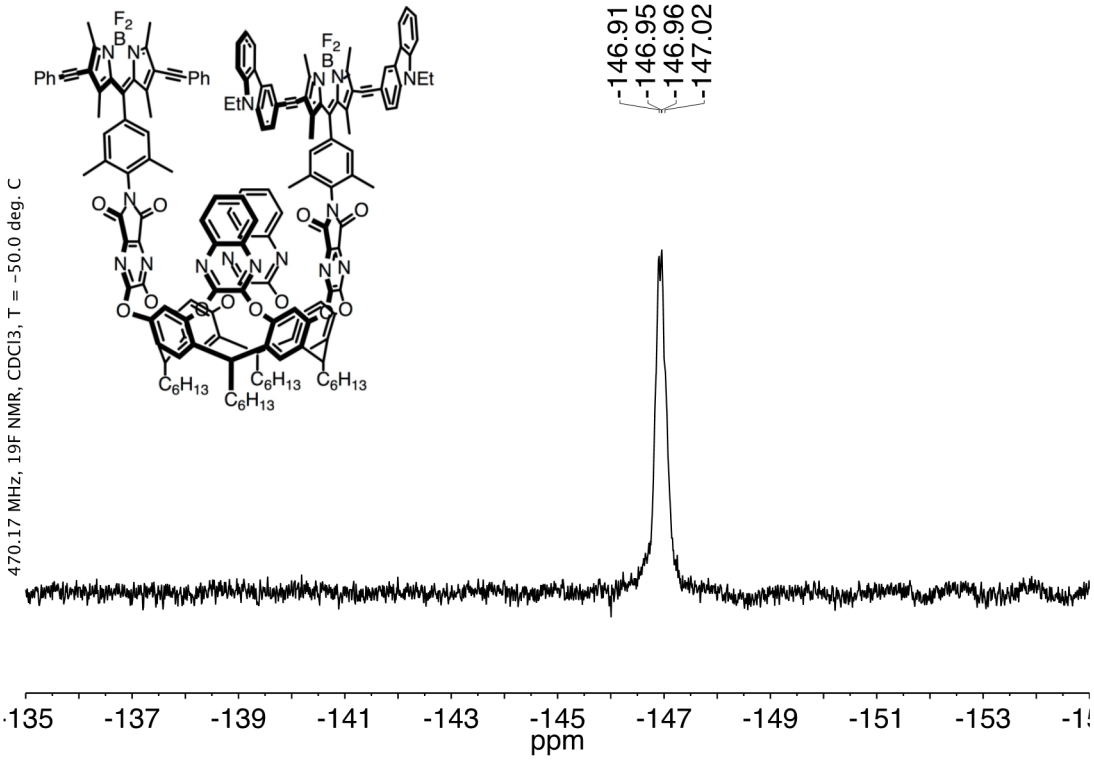

Figure S22. ^{19}F NMR spectrum (470 MHz) of cavitand **1**.

S2.2. Variable Temperature ^{1}H NMR Spectra of Cavitand 1

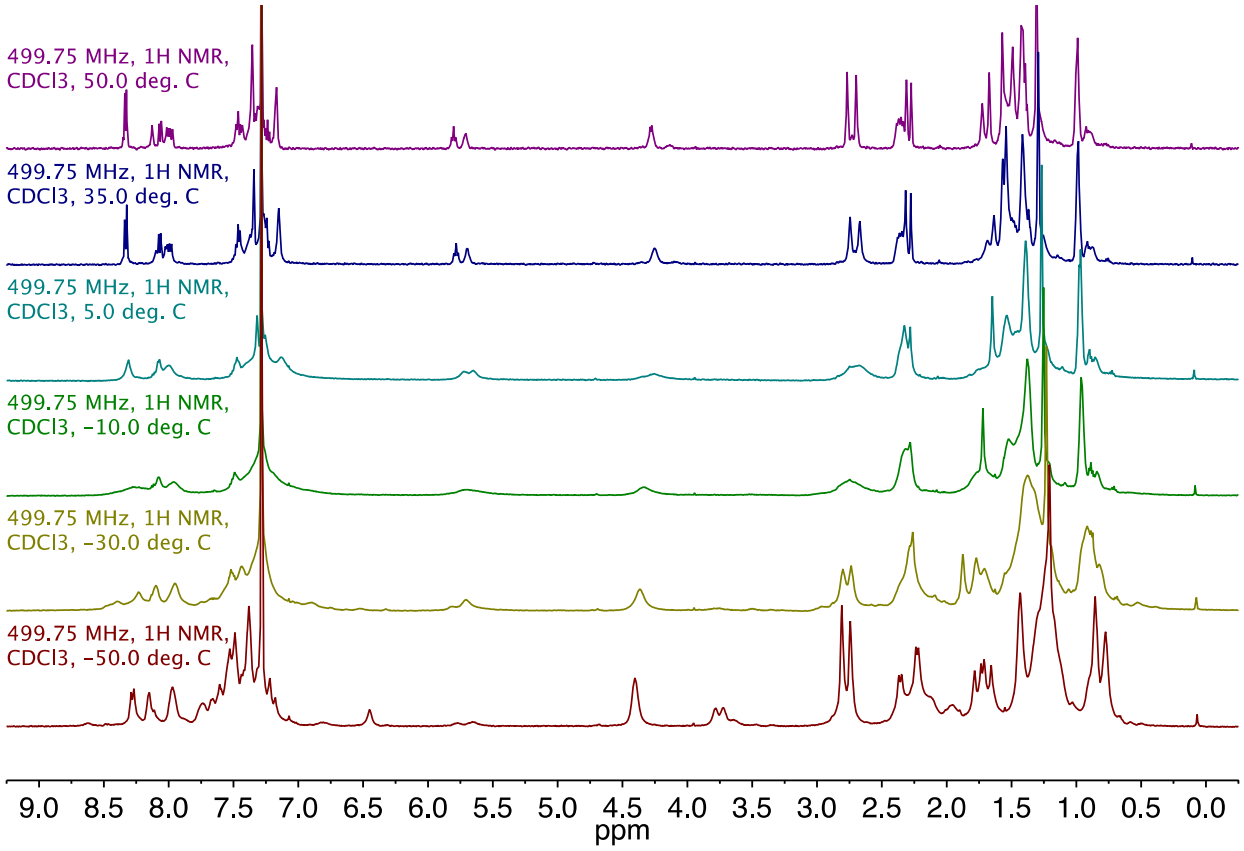

Figure S23. Variable temperature ^{1}H NMR spectra (500 MHz) of cavitand **1**.

S3. Absorption & Emission Spectra of Prepared Compounds

S3.1. Characterization Spectra of Donor Flap 2a, Acceptor Flap 2b, and Cavitand 1

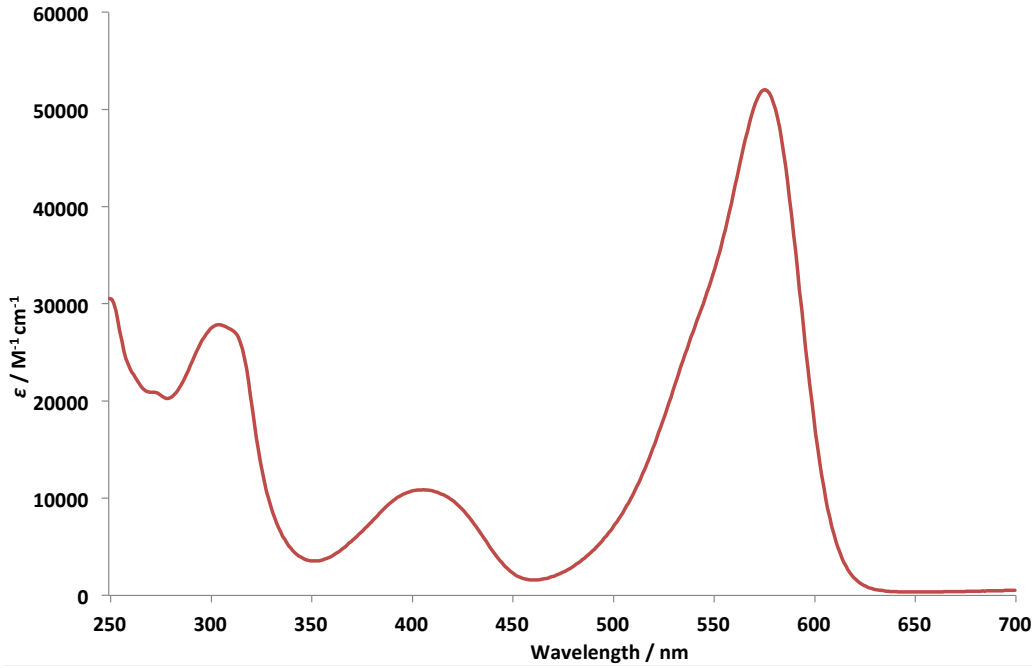

Figure S24. Absorption spectrum of donor arm **2a** in CH_2Cl_2 at 294 K ($c = 4.64 \times 10^{-5}$ M).

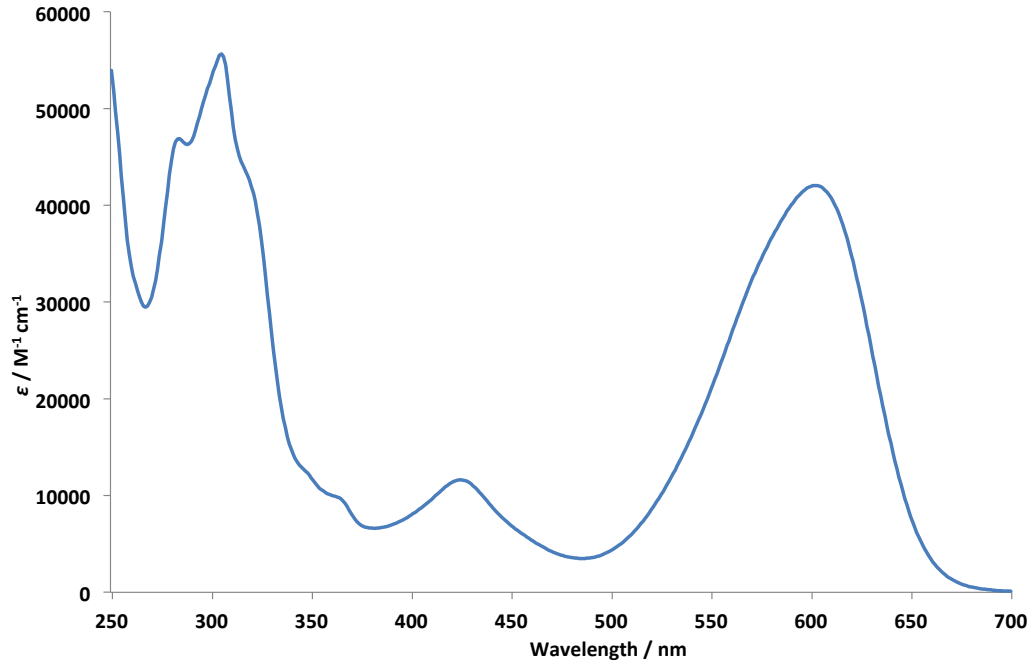

Figure S25. Absorption spectrum of acceptor arm **2b** in CH_2Cl_2 at 294 K ($c = 5.70 \times 10^{-5}$ M).

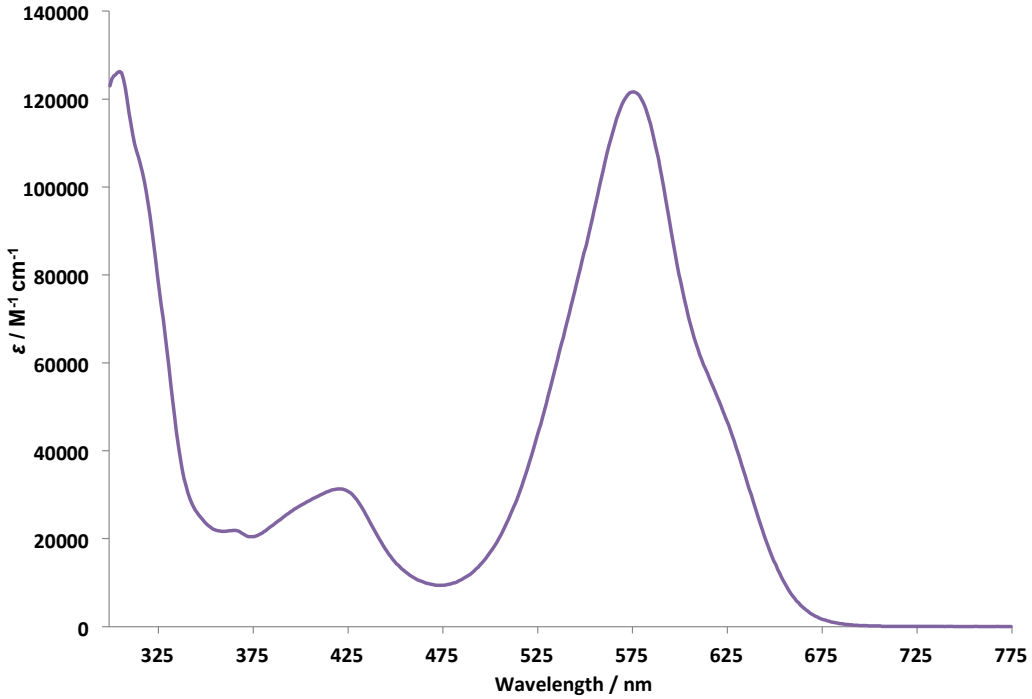

Figure S26. Absorption spectrum of cavitand **1** in $CHCl_3$ at 294 K ($c = 2.59 \times 10^{-5}$ M).

S3.2. Titration of Cavitand 1 with Trifluoroacetic Acid

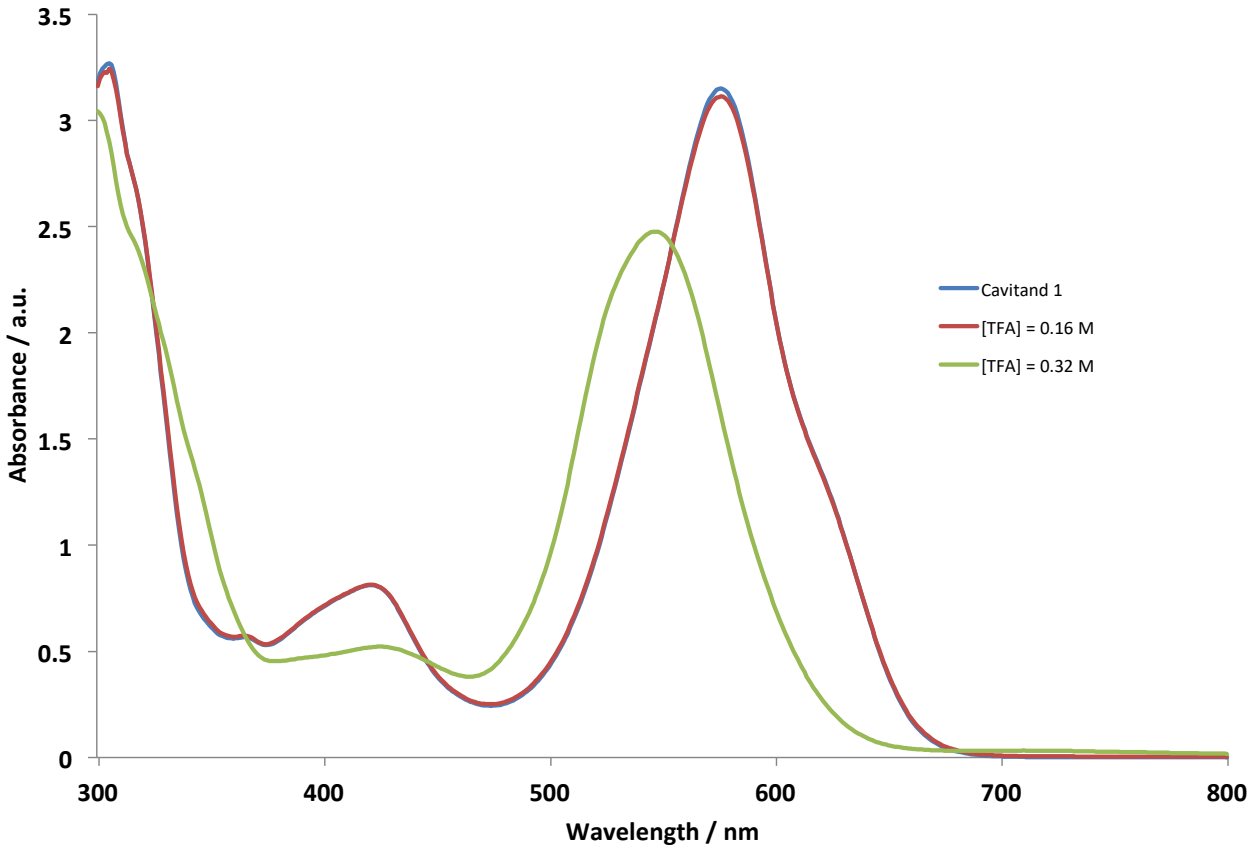

Figure S27. Absorption spectra of cavitand **1** in $CHCl_3$ at 294 K ($c = 2.59 \times 10^{-5}$ M) with different TFA concentrations, recorded 16–20 min after mixing.

S4. Quantum Yield Measurements

All spectra for the quantum yield measurement were recorded using a Horiba Fluorolog 3 with the Quanta-Phi integrating sphere attachment. Actual calculation of quantum yields was performed using the software packaged with the instrument, and the values are recorded below in Table TS1. Scatter-corrected absorption is determined by subtracting the scatter signal at from the fluorophore solution from that of a solvent blank, measured with the same excitation source. Scatter-corrected emission is similarly determined by subtracting solvent blank signal from the fluorophore emission spectrum. The ratio of integrated fluorophore emission counts to absorption counts defines the quantum yield. In this case, acceptor emission spectra are scaled by a factor of 1/100 to account for a 100x longer integration time due to weak signal.

Table TS1. **Fluorescence quantum yield of donor and acceptor.**

	QY (%)
Donor	30.59 ± 0.848
Acceptor	4.40 ± 0.026

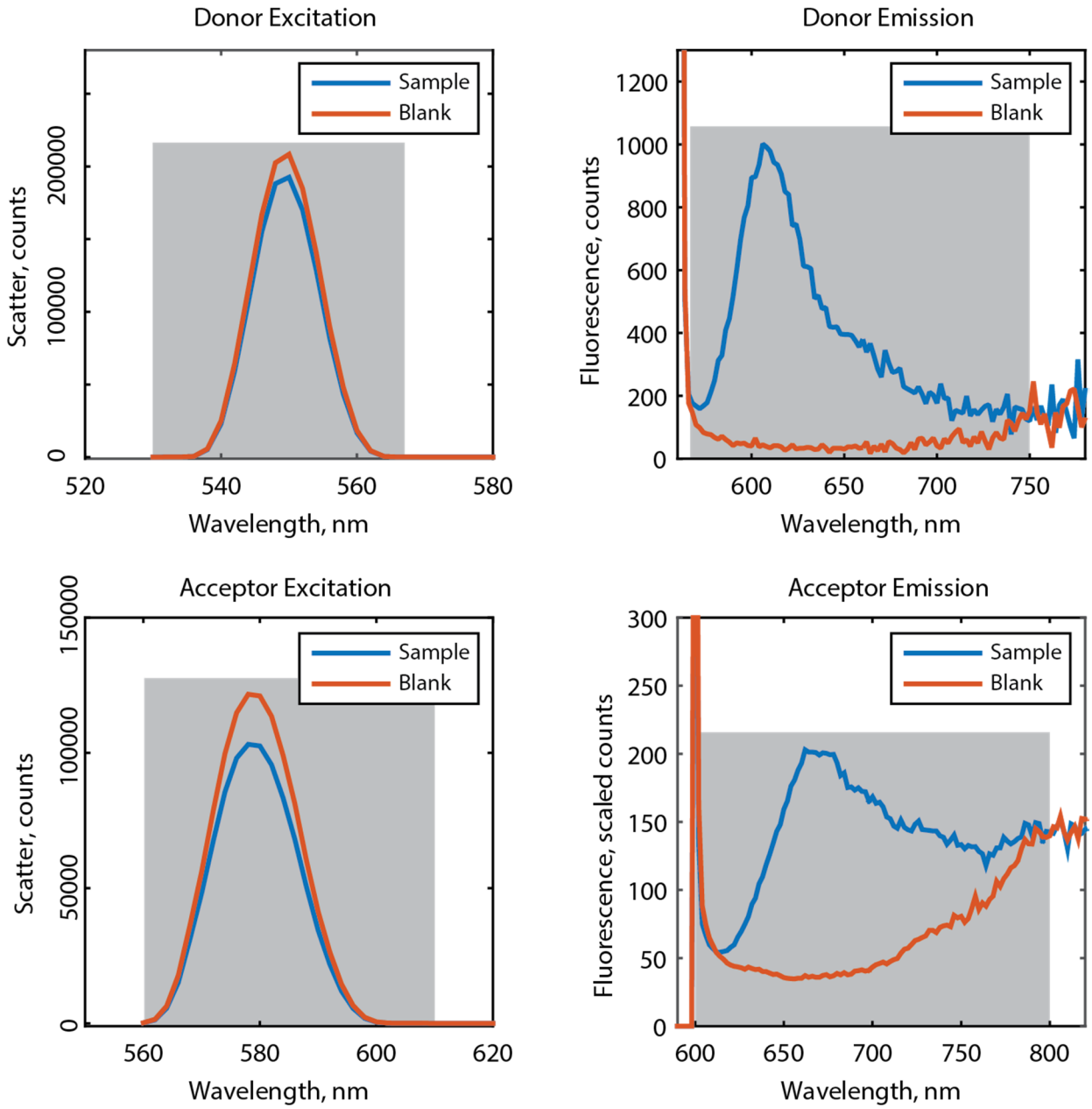

Figure S28. Excitation and Emission spectra (with reference solvent blank) for fluorescence quantum yield calculation. Grey boxes indicate bounds of integration for quantum yield calculations.

S5. Donor Fluorescence Lifetime Measurements

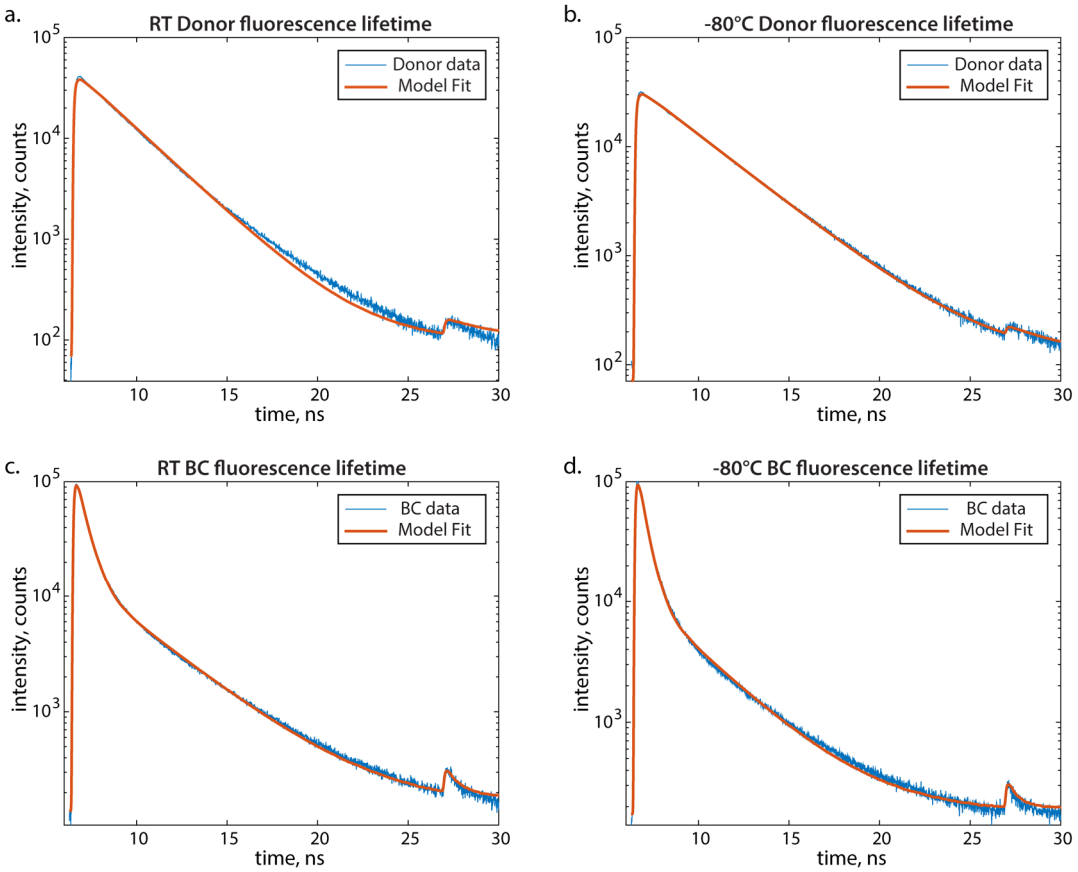

Figure S29. Fluorescence lifetimes measured by TCSPC. The measured data (in blue) are fitted to exponential decays convoluted with a measured instrument response function (in red) using software provided with the instrument. The jump at 27 ns is due to a small bleed through in the pulse picker used to control excitation pulse timing.

Table TS2. **Fluorescence lifetimes measured by TCSPC.**

	Temperature	τ_1 (ps)	τ_2 (ps)	E (%)
kite BC	193 K	411 ± 0.4	3090 ± 4	87.5± 0.1
vase BC	294 K	497 ± 0.6	3560 ± 4	78.0± 0.1
Donor	193 K	3300 ± 1	-	-
Donor	294 K	2600 ± 1	-	-

Multi-component exponential decay lifetimes were fit via a forward convolution method in the Vinci control and analysis software (ISS). The Instrument Response Function (IRF) was measured to be approximately 120 ps FWHM in a 1% scattering solution of Ludox LS colloidal silica. Efficiency was calculated using the formula $E=1-\tau_{DA}/\tau_D$, where τ_{DA} represents the decay lifetime of the donor in the presence of the acceptor (τ_1 from BC fits) and τ_D is the decay lifetime of the donor alone.[8]

S6. Dephasing Lifetime Determination

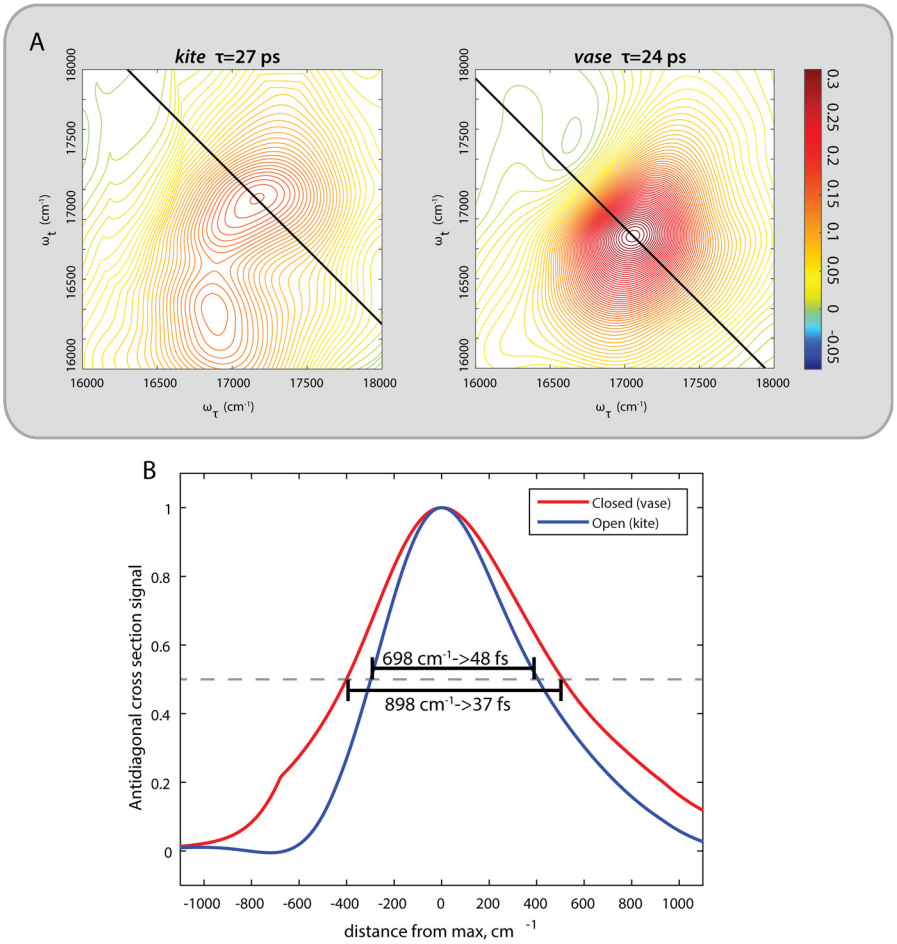

Figure S30. Dephasing lifetime derived from nonradiative relaxation signals. a) Nonradiative relaxation lifetime maps of *kite* and *vase* conformation. The figures are the same as Figure 3 in the main text, overlaid with location of antidiagonal cut, aligned with max signal. **b)** Antidiagonal profile with inset FWHM and corresponding dephasing lifetimes, calculated as the inverse of the frequency FWHM.[9]

S7. Stokes Shift

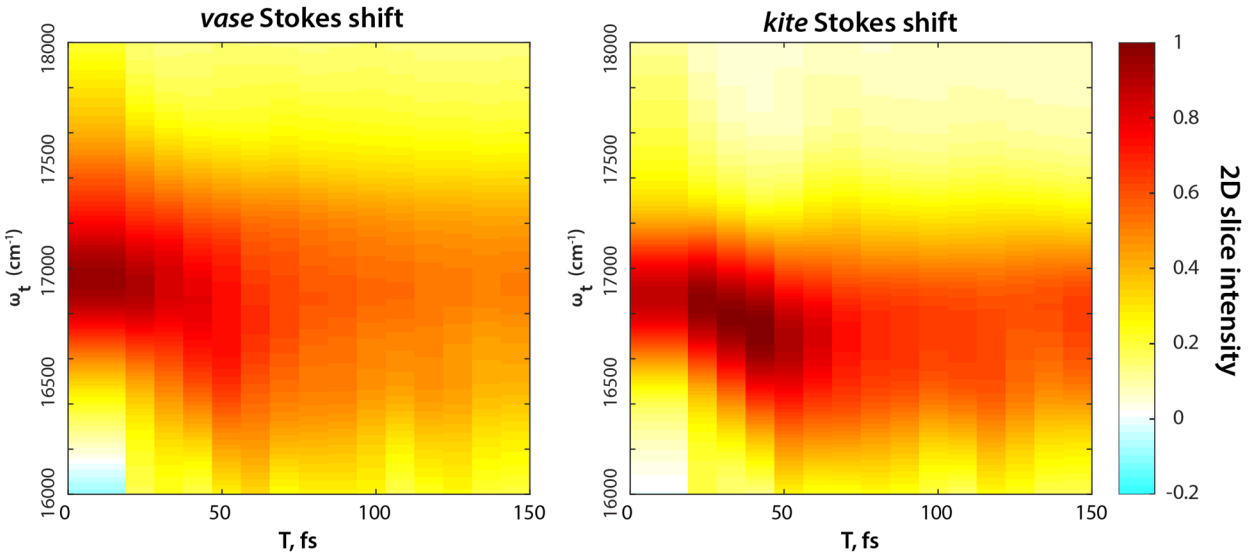

Figure S31. Stokes shift in *vase* and *kite* measured by ultrafast 2DES. Shown is a vertical slice of the 2D spectrum taken at ω_τ =17100 cm^{-1} from 0 to 150 fs waiting time. Vertical axis ω_t is the same as in all other 2D spectra shown. Initial excitations relax on the order of 30-50 fs, consistent with dephasing lifetimes calculated from Figure S30.

S8. Fluorescence Model

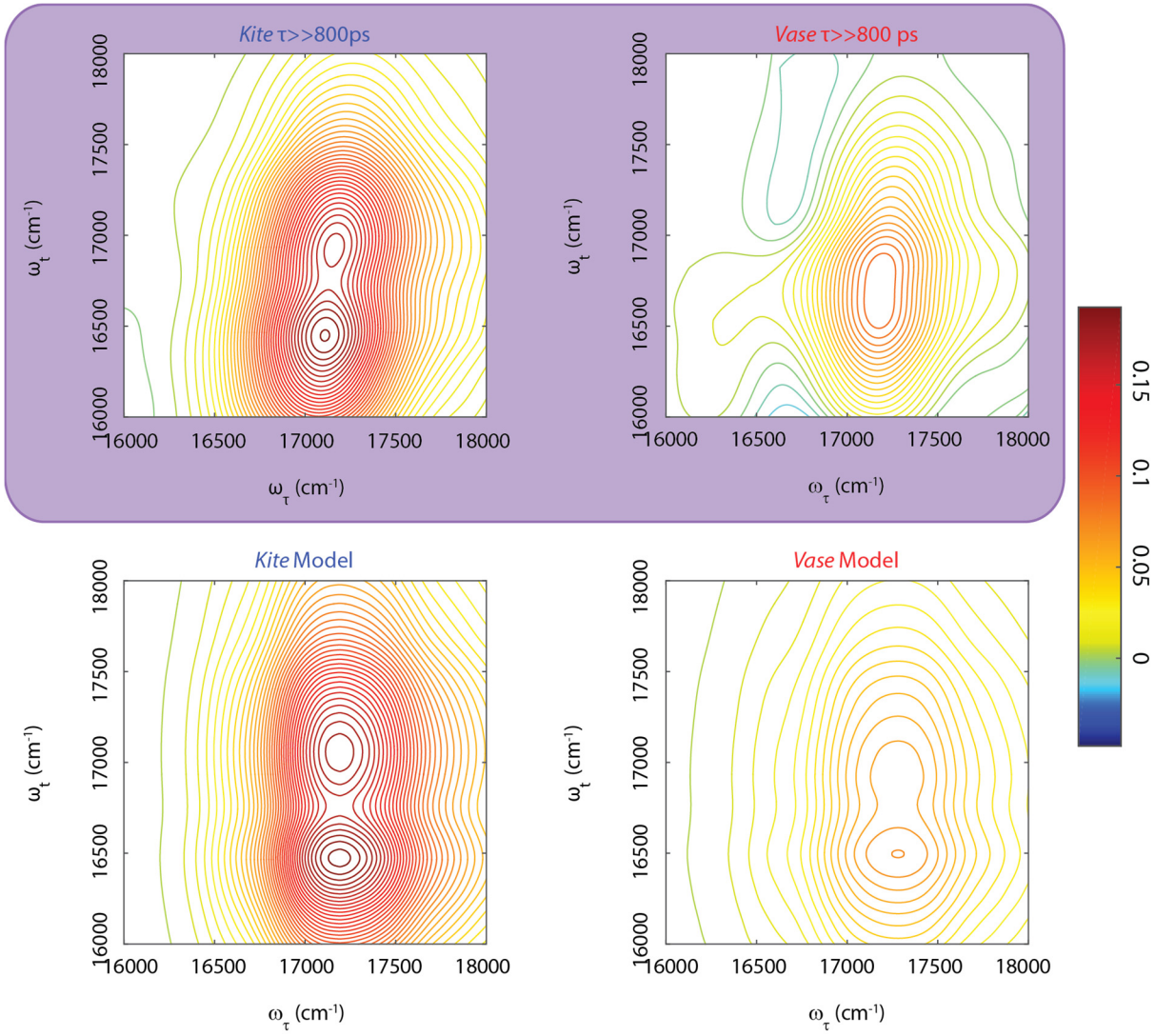

Figure S32. Comparison between residual fluorescence features in figure 3 with simulated spectra of donor. Top row shows long time lifetime maps for both *kite* (-80°C) and *vase* (RT) configurations. Bottom row shows simulated spectra made from a convolution of the donor absorption with the sum of the donor absorption and fluorescence.

Simulated spectra were also convoluted (twice in ω_τ and once in ω_t) with a measured laser spectrum to produce the expected 2D signal.

S9. Phasing

Phasing was performed as described in previous publications.[10-11] From the projection slice theorem, the real part of a 2D spectrum summed along ω_τ should match a symmetric pump-probe spectrum generated from the same light at the same waiting time. To correct for phase errors in our experimental setup, we fit the 2D spectra with an added phase function to pump probe data collected on a separate instrument. Our phase error is time independent, so all waiting times have the same phase correction applied. To further ensure comparable datasets, the same phase adjustments were applied to both the -80°C and RT datasets. The phase function applied includes a constant phase plus terms linear and quadratic in $\omega_t$and ω_τ.

$$S_{2D}{}^{phased} = a_1 S_{2D} e^{i\left(a_2 + a_3(\omega_t - \omega_{t,0}) + a_4(\omega_t - \omega_{t,0})^2 + a_5(\omega_\tau - \omega_{\tau,0}) + a_6(\omega_\tau - \omega_{\tau,0})^2\right)}$$

$$S_{pump\ probe} = \int \Re[S_{2D}{}^{phased}] d\omega_\tau$$

Pump probe spectra were recorded with a separate instrument, as described previously.[11] Ultrafast (fs-resolved) 2DES were used for phasing to pump probe, and the same phasing correction parameters were applied to all datasets. All 2D datasets were collected on the same instrument within a 36 hour period. Representative phased data from this short time experiment, as well as fitting results from phasing, are shown below.

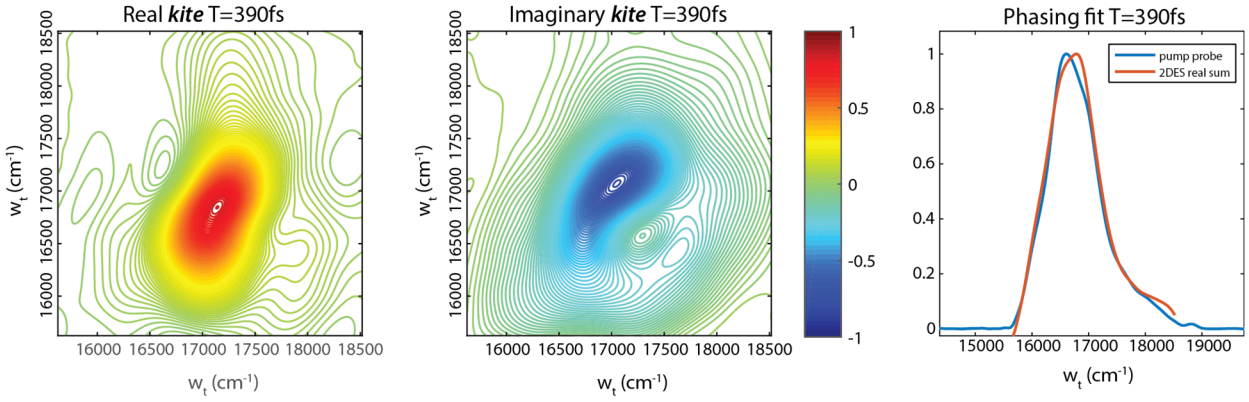

Figure S33. Representative phased data at T = 390 fs. The third plot shows the resulting fit of real value phased 2D data summed across ω_τ (2DES real sum, red) to the pump probe spectrum at the same waiting time (pump probe, blue).

S10. Fitting Algorithm

To obtain the lifetime maps shown in Figure 4, the following approach was taken: First, lifetimes were determined using a binned dataset (10x in both frequency dimensions) with waiting times from 5 ps to 800 ps. Time traces associated with each pixel in the 2D spectra were fit to a bi-exponential decay with an offset, e.g.

$$\boldsymbol{S(T) = A_1 e^{-T/\tau_1} + A_2 e^{-T/\tau_2} + A_3}$$

where $\boldsymbol{A_3}$ corresponds to the strength of a $\boldsymbol{\tau_3 = \infty}$ signal. Results of this fit were used to filter out points with less than 10% total signal from the first or second lifetime. The remaining signal was then least-squares fit to the same model, but with $\boldsymbol{\tau_1}$ and $\boldsymbol{\tau_2}$ constant across the dataset (to optimize those values). These lifetimes were then used to generate the maps shown in Figure 4 using an unbinned dataset. For this, each pixel in frequency space was normalized and least-squares fit to the same model with the global times. The resulting map of pre-exponentials (which summed to one in each pixel) was then weighted by the signal at T=5ps (the first nonzero waiting time) to give the plots in Figure 4. Confidence bounds for the pre-exponentials are shown in Figure S34, below. To generate the maps shown in Figure S34, we scaled one side of the 95% confidence bound for the given parameter by the intensity of the starting value (same scaling as in Figure 4 in main text).

Table TS3. **Lifetimes used to generate lifetime maps.**

	$\boldsymbol{\tau_1}$ **(ps)**	$\boldsymbol{\tau_2}$ **(ps)**
kite	24± 3	510±40
vase	27± 5	271±8

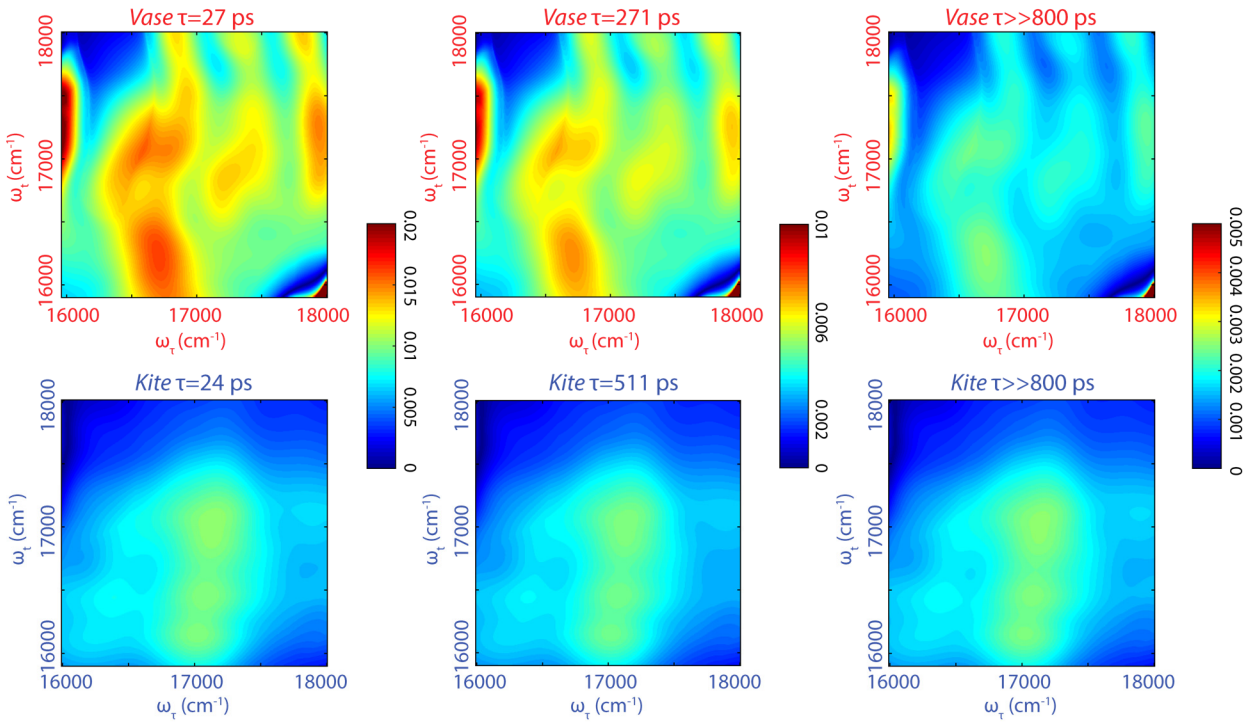

Figure S34. Absolute value of 95% confidence bounds for fitting maps presented in Figure 4 of the main text. Generated by multiplying one side of the symmetrical 95% confidence range of the relevant fit parameter (absolute value) with the starting real value signal as is done in Figure 4.

S11. Diagonal and Off-Diagonal Example Fits

Table TS4. Fit parameters with 95% confidence intervals for time traces shown in Figure S35.

diagonal	A_1	τ_1 (ps)	A_2	τ_2 (ps)	A_3
294 K	0.166 ± 0.017	20.2 ± 3.8	0.746 ± 0.007	260.9 ± 6.5	0.0586 ± 0.0045
193 K	0.229 ± 0.012	26.8 ± 2.8	0.568 ± 0.009	496.2 ± 28.6	0.165 ± 0.014

crosspeak	A_1	τ_1 (ps)	A_2	τ_2 (ps)	A_3
294 K	0.135 ± 0.033	39.5 ± 17.8	0.659 ± 0.027	286.0 ± 25.0	0.0649 ± 0.0127
193 K	0.153 ± 0.023	27.2 ± 8.0	0.501 ± 0.028	598.0 ± 93.5	0.152 ± 0.038

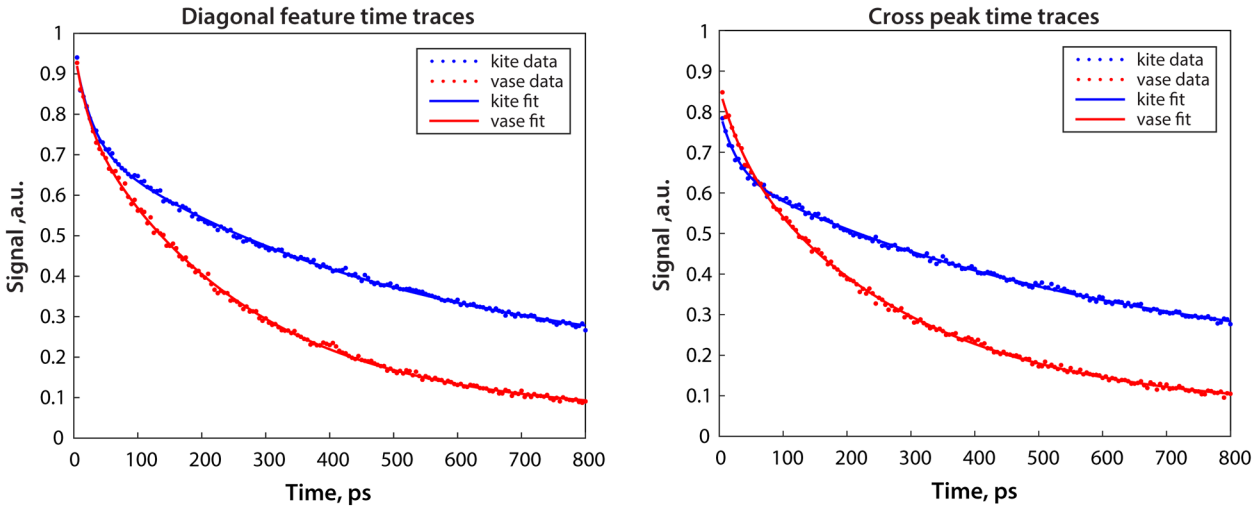

Figure S35. Representative time traces from the diagonal at 17100 cm^{-1} and at the cross peak at 17100 cm^{-1} and 16400 cm^{-1}. Fit parameters are listed in table TS4.

S12. 2D Spectral Data Shown in Figure 3

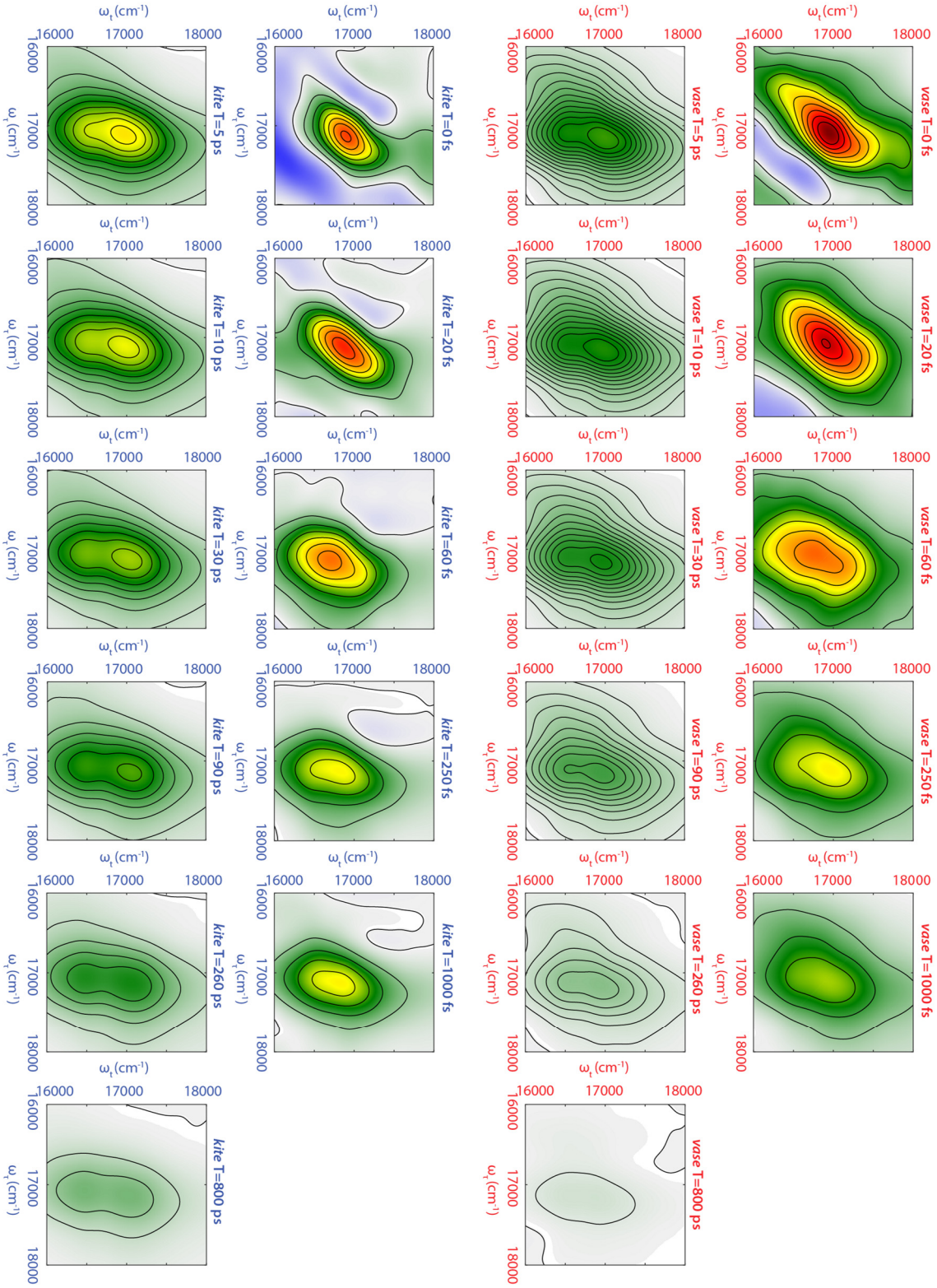

Figure S36. 2D spectral data shown in stacked form in Figure 3c.

S13. References

1. Pangborn, A. B.; Giardello, M. A.; Grubbs, R. H.; Rosen, R. K.; Timmers, F. J., Safe and Convenient Procedure for Solvent Purification. *Organometallics* **1996,** *15* (5), 1518-1520.
2. Hishikawa, K.; Nakagawa, H.; Furuta, T.; Fukuhara, K.; Tsumoto, H.; Suzuki, T.; Miyata, N., Photoinduced Nitric Oxide Release from a Hindered Nitrobenzene Derivative by Two-Photon Excitation. *Journal of the American Chemical Society* **2009,** *131* (22), 7488-7489.
3. Pochorovski, I.; Breiten, B.; Schweizer, W. B.; Diederich, F., FRET Studies on a Series of BODIPY-Dye-Labeled Switchable Resorcin-4-arene Cavitands. *Chemistry - A European Journal* **2010,** *16* (42), 12590-12602.
4. Kato, S.-I.; Shimizu, S.; Taguchi, H.; Kobayashi, A.; Tobita, S.; Nakamura, Y., Synthesis and Electronic, Photophysical, and Electrochemical Properties of a Series of Thienylcarbazoles. *The Journal of Organic Chemistry* **2012,** *77* (7), 3222-3232.
5. Azov, V. A.; Diederich, F.; Lill, Y.; Hecht, B., Synthesis and Conformational Switching of Partially and Differentially Bridged Resorcin[4]arenes Bearing Fluorescent Dye Labels. Preliminary Communication. *Helvetica Chimica Acta* **2003,** *86* (6), 2149-2155.
6. Cram, D. J.; Choi, H. J.; Bryant, J. A.; Knobler, C. B., Host-guest complexation. 62. Solvophobic and entropic driving forces for forming velcraplexes, which are 4-fold, lock-key dimers in organic media. *Journal of the American Chemical Society* **1992,** *114* (20), 7748-7765.
7. Castro, P. P.; Zhao, G.; Masangkay, G. A.; Hernandez, C.; Gutierrez-Tunstad, L. M., Quinoxaline Excision: A Novel Approach to Tri- and Diquinoxaline Cavitands. *Organic Letters* **2004,** *6* (3), 333-336.
8. Millington, M.; Grindlay, G. J.; Altenbach, K.; Neely, R. K.; Kolch, W.; Benčina, M.; Read, N. D.; Jones, A. C.; Dryden, D. T. F.; Magennis, S. W., High-precision FLIM–FRET in fixed and living cells reveals heterogeneity in a simple CFP–YFP fusion protein. *Biophysical Chemistry* **2007,** *127* (3), 155-164.
9. Hamm, P.; Zanni, M., *Concepts and methods of 2D infrared spectroscopy*. Cambridge University Press: Cambridge ; New York, 2011.
10. Flanagan, M. L.; Long, P. D.; Dahlberg, P. D.; Rolczynski, B. S.; Massey, S. C.; Engel, G. S., Mutations to R. sphaeroides Reaction Center Perturb Energy Levels and Vibronic Coupling but Not Observed Energy Transfer Rates. *The Journal of Physical Chemistry A* **2016,** *120* (9), 1479-1487.
11. Caram, J. R.; Zheng, H.; Dahlberg, P. D.; Rolczynski, B. S.; Griffin, G. B.; Dolzhnikov, D. S.; Talapin, D. V.; Engel, G. S., Exploring size and state dynamics in CdSe quantum dots using two-dimensional electronic spectroscopy. *The Journal of Chemical Physics* **2014,** *140* (8), 084701.